Segmental dynamics in polymers: from cold melts to ageing and stressed glasses

2009 J. Phys.: Condens. Matter 21 503101

(http://iopscience.iop.org/0953-8984/21/50/503101)

IOP Publishing Journal of Physics: Condensed Matter

J. Phys.: Condens. Matter **21** (2009) 503101 (20pp) doi:10.1088/0953-8984/21/50/503101

TOPICAL REVIEW

Segmental dynamics in polymers: from cold melts to ageing and stressed glasses

K Chen[1], E J Saltzman[2] and K S Schweizer[3]

Department of Materials Science, University of Illinois, 1304 West Green Street, Urbana, IL 61801, USA

E-mail: kschweiz@illinois.edu

Received 30 July 2009
Published 23 November 2009
Online at stacks.iop.org/JPhysCM/21/503101

Abstract

Recent progress in developing statistical mechanical theories of supercooled polymer melts and glasses is reviewed. The focus is on those approaches that are either explicitly formulated for polymers, or are applications of more generic theories to interpret polymeric phenomena. These include two configurational entropy theories, a percolated free volume distribution model, and the activated barrier hopping nonlinear Langevin theory. Both chemically-specific and universal aspects are discussed. After a brief summary of classic phenomenological approaches, a discussion of the relevant length scales and key experimental phenomena in both the supercooled liquid and glassy solid state is presented including ageing and nonlinear mechanical response. The central concepts that underlie the theories in the molten state are then summarized and key predictions discussed, including the glass transition in oriented polymer liquids and deformed rubber networks. Physical ageing occurs in the nonequilibrium glass, and theories for its consequences on the alpha relaxation are discussed. Very recent progress in developing a segment scale theory for the dramatic effects of external stress on polymer glasses, including acceleration of relaxation, yielding, plastic flow and strain hardening, is summarized. The article concludes with a discussion of outstanding theoretical challenges.

(Some figures in this article are in colour only in the electronic version)

Contents

[1] Present address: Materials Research Laboratory, University of California, Santa Barbara, CA, USA.
[2] Present address: Department of Chemical Engineering, Columbia University, NY, USA.
[3] Author to whom any correspondence should be addressed.

1. Introduction

Dense polymeric liquids and amorphous solids are a vast class of materials of exceptional technological significance [1–4]. In most cases, chemical synthesis results in quenched disorder at the single chain level which precludes crystallization and hence glasses unavoidably form upon cooling. Polymers are characterized by high chemical diversity on local scales, and (quasi) universal features on intermediate and longer length scales [5–7]. In most applications, polymer glasses are used at temperatures close to the kinetic glass transition temperature, T_g, and hence nonequilibrium physical ageing is of paramount importance [2, 8]. The nonlinear mechanical response to applied stress is a fascinating problem in nonequilibrium statistical physics, which is of critical engineering relevance and has been experimentally studied in depth [2, 4, 9]. In the literature and at international glass dynamics meetings one often hears the opinion expressed that 'polymers are different' or 'too complicated'. We disagree, and believe the rich glassy phenomena exhibited by these materials provide an exceptional opportunity for fundamental scientific inquiry within the context of condensed matter physics.

To set the stage for the discussion of dynamics, we first summarize the chemical complexities of polymers and relevant equilibrium features. Long chain molecules are characterized by structure on multiple length scales, and in both theoretical and simulation studies some coarse graining is unavoidable. Figure 1 illustrates this in the context of a polyethylene chain. There are several 'chemical' (Angstrom) length scales at the monomer level (diameter d < nm). Rotational isomerism [5] results in randomization of the chain backbone beyond a material-specific, but weakly temperature-dependent, persistence (l_p) or Kuhn (l_K) length, typically of order ∼0.6–1.5 nm. These backbone stiffness correlation lengths are given by [5]:

$$l_K \simeq 2l_p \approx C_\infty l_b. \tag{1}$$

The required structural parameters in equation (1) are usually defined via the macromolecular mean square end-to-end distance: $\langle R^2\rangle = N_{bb}C_N l_b^2$, where C_N (typically ∼4–10) is the material-specific characteristic ratio, N_{bb} the number of backbone bonds, and l_b an average chemical bond length. The characteristic ratio typically increases with N_{bb}, saturating at a chemically-specific degree of polymerization. These stiffness length scales have qualitatively the same physical meaning as the 'statistical segment length', σ, beyond which the polymer is a flexible random walk. The definition of the latter is not unique. To reproduce equilibrium single chain correlations

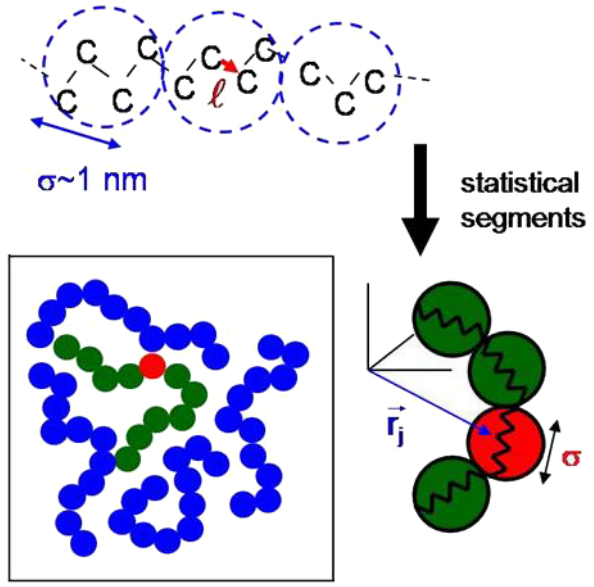

Figure 1. Illustration of coarse graining of a polyethylene chain, showing encapsulation of local structure within statistical segments of size σ. Inset: schematic of a polymer melt at the segmental scale. Slow dynamics results from the forces exerted on a tagged segment (red; light) by nearby segments on different chains (blue; dark).

on intermediate 'self-similar' length scales ($d \ll r \ll R_g$) requires

$$\sigma = \sqrt{C_\infty} l_b \tag{2}$$

where $\langle R^2\rangle = N\sigma^2$, N is the number of segments, and C_∞ is the long chain limit of C_N. The collective density fluctuation correlation length in polymer liquids is similar to small molecule fluids [10], $\xi_\rho \sim d$.

Segment scale relaxation has a fast (beta) component, and a much slower alpha process which is the focus of this article. The alpha relaxation in polymers is independent of chain length in the $N \gg 1$ limit. It sets the timescale for even slower dynamical motions associated with chain connectivity (figure 1) and uncrossability (entanglement) which depend explicitly on N [5–7]. In contrast to other glassy materials, the alpha relaxation does not determine macroscopic diffusion and viscosity. However, all the other aspects of glassy materials composed of small elementary units [11] are relevant to polymers, including average properties (e.g., alpha relaxation time and characteristic temperatures, and their chemistry, pressure and chain length dependences) and dynamic fluctuation phenomena (e.g., nonexponential relaxation, decoupling effects). Cold polymer melts are characterized by a remarkably broad variation of behavior for all these aspects. The ability to tune macromolecular size allows the unique opportunity to probe dynamic heterogeneity as a function of time and length scale at *fixed* chemistry and intermolecular forces. The focus of this article is recent theoretical progress relevant to slow segmental dynamics in bulk, homogeneous, one-component polymer liquids and glasses.

1.1. Classic phenomenological approaches

Two venerable phenomenological approaches are widely employed to interpret glassy polymer relaxation. One is the 'free volume' model (FVM) based on kinetic blocking where mobility requires the accumulation of a critical amount of 'open space' via 'diffusing defects'. Unfortunately, free volume is ill-defined and not directly measurable. Based on simple assumptions about the temperature dependence of the free volume, the mean alpha relaxation time is [11, 12]:

$$\frac{\tau_\alpha}{\tau_0} = \exp\left(b\frac{V}{V_f}\right) \qquad lg\left(\frac{\tau_\alpha}{\tau_0}\right) \simeq \frac{-C_1(T - T_{\rm ref})}{T - T_0} \tag{3}$$

where τ_0 is an elementary timescale, b a number of order unity, V ($V_{\rm f}$) the molar (free) volume, C_1 a nonuniversal parameter, $T_{\rm ref}$ a reference temperature (typically $\sim T_{\rm g}$), and at $T_0 > 0$ the free volume vanishes and the relaxation time diverges in an essential singularity manner. Polymer-specific aspects enter only implicitly and empirically.

A second class of theories is centered on the thermodynamic configurational entropy often, but not always, supplemented with a literal entropy crisis or catastrophe at a nonzero Kauzmann temperature [1, 11], $S_{\rm c}(T = T_{\rm K}) \to 0$. Adams and Gibbs (AG) postulated this entropy determines the alpha relaxation time as [11, 13]:

$$\tau = \tau_0 \exp\left[\beta\Delta\mu\frac{S_{\rm c}^*}{S_{\rm c}(T)}\right] \tag{4}$$

where $\beta = 1/k_{\rm B}T$ is the inverse thermal energy, and $\Delta\mu$ ($S_{\rm c}^*$) is the high-temperature non-collective activation energy (configurational entropy). If $S_{\rm c}(T)$ is approximated as a linear function of temperature, then the classic Vogel–Fulcher–Tamman (VFT) result follows:

$$\tau_\alpha = \tau_0 \exp\left(\frac{DT_{\rm K}}{T - T_{\rm K}}\right) \tag{5}$$

which is the same form as the FVM if one identifies $T_{\rm K} = T_0$. Dynamics is activated with a barrier proportional to the number of elementary units $z^* = S_{\rm c}^*/S_{\rm c}(T)$ that move simultaneously in a cooperatively rearranging region (CRR). What constitutes an 'elementary unit' is fundamentally ambiguous since theories invoke, to varying degrees, some coarse graining, and a precise definition of 'cooperativity' is absent. The literal entropy crisis approach was worked out in great detail for simple lattice models by diMarzio and co-workers [14–16] based on the assumption that $T_{\rm K}$ is a direct indication of the laboratory $T_{\rm g}$. Configurational entropy is particularly hard to define for polymers given the many intrachain degrees of freedom and the usual nonexistence of a crystalline reference state.

The vast majority of physical ageing theories for polymer glasses are highly phenomenological [11, 12]. Perhaps the most famous is the Tool–Narayanaswamy–Moynihan (TNM) model [17], which can provide good fits of some measurements based on adjustable parameters such as the fictive temperature and 'nonlinearity parameter'. A first order kinetic equation is typically postulated for a structural or thermodynamic variable (e.g., configurational entropy, free volume) that is assumed to control segmental relaxation, which then results in a nonequilibrium time evolution of the relaxation time.

The phenomenological Eyring model is still widely employed as a conceptual and fitting framework for describing stress-induced yielding and nonlinear mechanical response in polymer glasses [4, 9, 18]. It assumes τ_α reflects a simple *Arrhenius* activated hopping process (potential energy $E_{\rm A}$) of an undefined elementary unit. Applied stress (τ) results in a *linear* reduction of the barrier of a mechanical work form:

$$\tau_\alpha(T, \tau) = \tau_0 \exp[(E_{\rm A} - \tau V^*)/k_{\rm B}T] \tag{6}$$

where V^* is a temperature-*independent* 'activation volume'. The dynamic yield stress, $\tau_{\rm y}$, signals a mechanically-induced 'solid-to-liquid' transition resulting in irreversible (local for polymers) plastic flow identified as when $\tau_\alpha(T, \tau_{\rm y}) \approx \dot\gamma^{-1}$. Equation (6) combined with the latter condition results in an explicit expression for the yield stress:

$$\tau_{\rm y} = \frac{E_{\rm A}}{V^*} + \frac{k_{\rm B}T}{V^*}\ln(\dot\gamma\tau_0). \tag{7}$$

Equation (7) predicts: (i) the rate-independent contribution to the yield stress is a temperature-independent material constant, (ii) the temperature and strain rate dependences enter in a multiplicative fashion, and (iii) $\tau_{\rm y}$ grows linearly with temperature and logarithmic strain rate. The Eyring model has been applied to essentially all glass forming materials; polymer-specific aspects enter only empirically via its three adjustable parameters.

Experimental and simulation studies have raised serious concerns about the Eyring model for glassy polymers [9, 19–23]. For example, (a) the extracted values of V^* vary enormously ($\sim$1–20 nm^3) with no structural correlation, (b) the activation volume depends on stress or strain, (c) the strain rate dependence of $\tau_{\rm y}$ is nearly temperature independent or gets stronger with cooling, and (d) the rate-independent contribution to $\tau_{\rm y}$ is not temperature independent but rather increases with cooling. The yielding behavior of polymer glasses is also sensitive to physical ageing which is not included in the Eyring model. At ultra-high strains polymers undergo massive conformational deformations, resulting in a large stress increase in the post-yield regime due to 'strain hardening' [4, 9] which the Eyring model does not address. Classic theories of strain hardening are based on ideal entropic rubber elasticity models [24] which appear to be fundamentally flawed (see sections 2.4 and 7.3).

1.2. Modern theories

This topical review focuses solely on recent theories formulated for *deeply* supercooled polymer liquids and glasses; we also discuss two generic models that have been explicitly applied to interpret polymeric phenomena. Interesting approaches not covered include the potential energy landscape paradigm [25, 26], ideal mode coupling theory (MCT) [27, 28], elastic shoving models [29], shear transformation zone theory [30], kinetically constrained models [31, 32], and the soft glassy rheology model [33]. We consider four

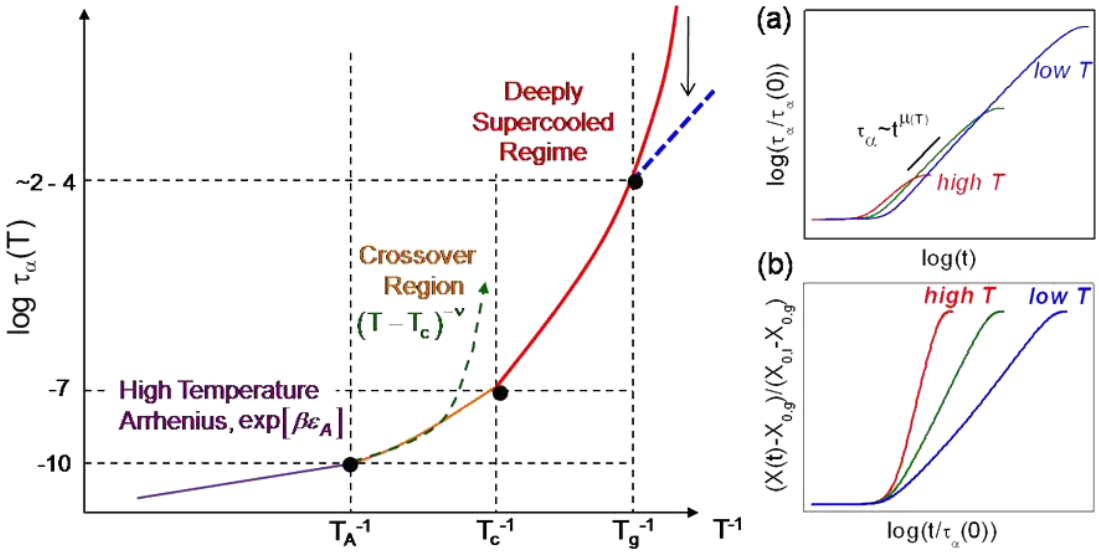

Figure 2. Schematic alpha relaxation time as a function of inverse temperature. The four regimes of relaxation are: high-temperature Arrhenius (purple), crossover (orange) (green), deeply supercooled regime (red), and nonequilibrium glass regime (blue). Boundaries between regimes are demarcated by characteristic times and temperatures. Inset: schematic logarithmic time evolution in the ageing glass of the normalized: (a) alpha relaxation time, and (b) thermodynamic and mechanical properties.

approaches: (1) random first order transition (RFOT) theory [34], (2) lattice cluster entropy theory (LCET) [35], (3) percolated free volume distribution (PFVD) model [36], and (4) the nonlinear Langevin equation (NLE) activated barrier hopping theory [37]. The degree of coarse graining, and extent to which the polymer-specific aspects are accounted for, varies widely among these theories. Both the RFOT [34] and LCET [35] have been reviewed in great depth recently, and hence their basic elements are more briefly discussed.

In section 2, key aspects of the experimental phenomenology are summarized. Basic elements of the theoretical approaches in the equilibrated liquid are discussed in section 3. Section 4 briefly addresses how these approaches treat heterogeneous dynamics. The effect of spatial anisotropy in deformed rubbers and oriented melts is the subject of section 5. Section 6 discusses nonequilibrium relaxation and physical ageing in the glass. Extension of the polymeric NLE theory to nonlinear mechanical behavior is the subject of section 7. The article concludes with a future outlook in section 8.

2. Experimental phenomenology

Excellent reviews exist of the experimental behavior of cold polymer melts and glasses [1, 3, 8, 9, 38]. Here we summarize key observations.

2.1. Generic relaxation phenomena

Segmental relaxation can be probed via dielectric spectroscopy, NMR, dynamic light scattering, stress relaxation and other methods, all of which are quantitatively similar and show essentially identical temperature dependences [1, 11]. The overall behavior is qualitatively the same as for other glass forming materials, and a typical relaxation map for fragile liquids is sketched in figure 2. At high enough temperatures ($T > T_A$) an Arrhenius dependence is often observed, $\tau_\alpha(T) = \tau_0 \exp(\varepsilon_A/k_B T)$, where the activation energy depends on cohesive energy and chain stiffness [39]. Over a narrow intermediate temperature range, $T_B \sim T_c < T < T_A$, a rather weak non-Arrhenius behavior emerges for a few orders of magnitude of relaxation time which can be fit to various forms, e.g., the MCT critical power law [27] $\tau_\alpha(T)/\tau_0 \propto (T - T_c)^{-\Delta}$, or the VFT equation (5). Relaxation times at T_A and T_c are roughly material insensitive ($10^{-10\pm1}$ s [40] and $10^{-7\pm1}$ s [41], respectively), although this is debatable [3]. At the lower temperatures that define the deeply supercooled regime, $T_g < T < T_c$, a steep dependence is observed over many orders of magnitude which can usually be fit by a VFT equation or the Bassler–Ferry law [42]:

$$\tau_\alpha(T)/\tau_0 = \exp[(T^*/T)^2]. \tag{8}$$

The steepness of the temperature dependence is quantified by dynamic fragility

$$m \equiv \frac{\mathrm{d}}{\mathrm{d}(T_g/T)} \lg[\tau_\alpha(T)]|_{T=T_g}. \tag{9}$$

The fragility and temperature ratios, T_A/T_g or T_c/T_g, vary over an exceptionally wide range for different polymers [11, 43]. The singularities at T_K or T_0 deduced by large extrapolation typically lie 30–80 K below T_g [44]. Time correlation functions that probe segmental relaxation are highly stretched and can be fit by the KWW expression

$$C(t) = \exp[-(t/\tau_\alpha^*)^{\beta_K}]. \tag{10}$$

The stretching exponent usually decreases with cooling in a material-specific fashion, and for polymers is quite small at T_g [43, 45], $\beta_K \sim 0.25$–0.5. Even at high temperature the relaxation can be nonexponential due to chain connectivity induced intra-polymer cooperativity [5, 7].

Below T_g the alpha relaxation time generally crosses over to an Arrhenius form (figure 2). For polymers, the apparent activation energy decreases by typically a factor of ∼2–4 across T_g [46].[4] The common interpretation is the Arrhenius behavior in the glass is a nonequilibrium effect given the observation of physical ageing.

2.2. Polymer-specific liquid phenomena

On the most local scales, two highly nonuniversal features are relevant to segmental relaxation: (i) variable monomer shape and chemical identity associated with the backbone repeat unit and (if present) sidegroups, and (ii) chain backbone stiffness characterized by a persistence length which can vary by a factor of ∼3–4. A simplifying feature is most synthetic polymers interact primarily via van der Waals attractions. Nevertheless, dynamic fragility at T_g varies from $m \sim 45$ to >200 in amorphous polymers, and can be as low as ∼20 for semicrystalline polymers, a fragility range not observed in any other material class [11]. This breadth of behavior also applies to T_g, which varies from ∼150 K to nearly 500 K. Present experimental understanding of these chemical variations is as follows [44, 47–49]. (i) Polymers with very stiff backbones have a high T_g and fragility. (ii) Polymers with highly flexible backbones and no sidegroups have low T_g and fragility. (iii) If sidegroups become sterically bulky and/or relatively rigid, then polymers with flexible backbones become dynamically fragile and have a higher T_g. The lowest fragility occurs when the backbone and sidegroup stiffness are very similar.

At fixed chemical structure, glassy polymer dynamics depends on the degree of polymerization, N, in a finite size manner which saturates at a material-specific value. Typically, T_g and fragility monotonically increase with N [48]. The origin of this N dependence is subtle since conformational, interchain packing, and thermodynamic properties all vary in a finite size manner; e.g., density and characteristic ratio increase with N, while the compressibility decreases.

Based on mechanical measurements, the crossover to the deeply supercooled regime in polymer melts was historically called a 'liquid–liquid phase transition' [50] at a characteristic temperature T_{ll} typically ∼15–25% above T_g. Recent experiments find this temperature is close to estimates of the empirically-deduced dynamical crossover (MCT) T_c that signals the onset of the strongly activated dynamics regime [51, 52]. Hence, the true meaning of T_{ll} is that it indicates the emergence of transient segmental localization and a strong elastic response which is of practical materials processing importance.

Segmental scale dynamic heterogeneity has been probed using multi-dimensional NMR to extract a length scale, ξ_h, near T_g. Experiments have been performed on one polymer, polyvinylacetate, for which $\xi_h \sim 3.5$ nm [53].

The macromolecular end-to-end vector relaxation time, τ_{ee}, is also measurable. Far enough above T_g its temperature dependence is the same as local segmental relaxation leading to 'time-temperature superposition' (TTS) [44, 49], a form of dynamical slaving or homogeneity. However, in the deeply supercooled regime ($T < T_c$), nonuniversal deviations increasingly emerge with τ_{ee} exhibiting a slower increase with cooling relative to its segmental analog, with deviations at T_g varying from a factor of ∼3 to >100 in a manner that correlates with segmental dynamic fragility [54]. This uniquely polymeric phenomenon can be viewed as heterogeneous 'decoupling' of segmental and chain scale dynamics which can be expressed as a fractional Stokes–Einstein law:

$$\tau_{ee}(T)/\tau_\alpha(T) \propto [\tau_\alpha(T)]^{-\varepsilon} \tag{11}$$

where the exponent [54] varies over a very wide range, $\varepsilon \sim 0.15$–0.53. Until very recently [54], only tentative phenomenological attempts [44, 55] have been made to understand this striking phenomenon. Experiments have also shown that the dynamic fragility associated with macromolecular relaxation is generally both smaller in magnitude, and less nonuniversal, than its segmental counterpart [49, 54].

A distinguishing feature of polymers is they can exist in anisotropic states such as a deformed rubber network or oriented liquid crystal. Such organizational states are characterized by a segment orientational order parameter (τ_{or}) and anisotropic macromolecular dimensions (see figure 3). For crosslinked rubbers, T_g increases upon extension or compression [38]. Nonuniversal shifts of T_g (up or down) are observed in polymer thin films, but these represent even more complicated systems due to the presence of interfaces and confinement [56].

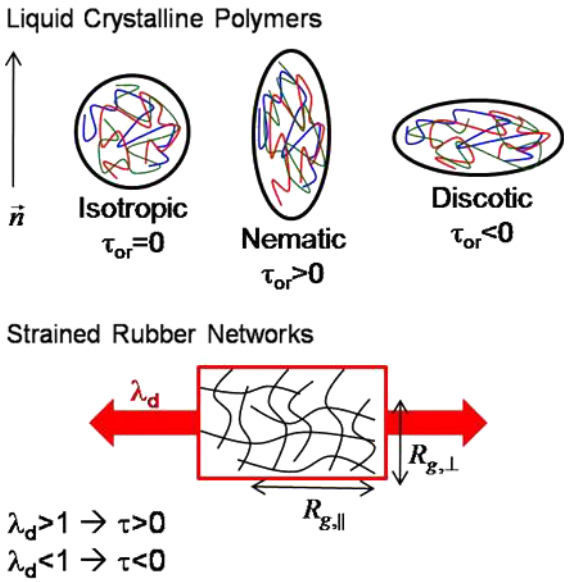

Figure 3. Illustration of anisotropy in bulk polymers for liquid crystals and strained rubber networks. The segmental orientational order parameter is denoted as τ or τ_{or}, and the macroscopic linear deformation ratio is denoted as λ_d.

2.3. Physical ageing

Below T_g a slow approach to equilibrium occurs known as physical ageing. This process is characterized by a waiting or ageing time (t_{age}) dependence of thermodynamic, relaxation

[4] See [46] for a detailed summary of the different measurements of apparent activation energy changes of polymer melts across the glass transition.

and mechanical properties. Properties evolve towards a more solid-like response [2, 8], e.g., the alpha time or elastic modulus (diffusion constant) increases (decreases) with t_{age}. Ageing is particularly important for polymer glasses since they are used at temperatures often only modestly below T_g. The temporal evolution of all properties is sigmoidal [8], although the short and long time behaviors are usually not experimentally accessible (figure 2). In the commonly observed intermediate regime, thermodynamic properties evolve roughly logarithmically with ageing time, while relaxation times grow as an apparent power law ($\sim t_{age}^{\mu}$). The ageing exponent, μ, generally increases with cooling, approaching unity sufficiently below T_g, but then usually drops rather abruptly at a polymer-specific large degree of undercooling [2]. The approach to equilibrium is 'asymmetric' since the waiting time evolution depends on whether the experimental protocol corresponds to an up or down temperature jump.

2.4. Linear and nonlinear mechanical response

Above T_g, the primary mechanical property studied is the linear glassy shear (G') modulus. However, at the experimentally accessible timescales it is often unmeasurably small, and 'turns on' rapidly as T_g is approached from above with $G' \sim$ GPa at the glass transition. Below T_g, the modulus increases much more weakly as roughly a linear function of temperature akin to a solid-like response [4, 9].

A primary scientific and engineering interest below T_g is the nonlinear mechanical response, and the complex phenomena of yielding, rejuvenation, plastic flow, and strain hardening [2, 4, 9, 24]. In a constant strain rate experiment, stress is measured as a function of strain for various temperatures, strain rates and ageing protocols. A typical response is shown in figure 4, and four regimes are usually observed. (1) Linear elastic response at low strain with a temperature-dependent modulus of order a GPa. (2) A local (yield) stress maximum, indicating 'strain softening' at strains $\gamma \sim$ 2–10%. (3) A 'plastic flow' regime where a plateau yield stress (∼10–100 MPa typically) emerges that is nearly independent of strain but depends strongly (weakly) on temperature (strain rate). (4) At very large strains, polymers massively deform and the stress rises sharply leading to 'strain hardening' which is of great practical importance with regards to avoiding fracture, shear banding, crazing and other failure mechanisms [4, 24]. The yield stress and hardening modulus both increase with cooling and strain rate.

If a mechanical test is done very quickly after a quench, physical ageing and so-called rejuvenation effects can be avoided [9]. The resulting stress–strain curve has all the same qualitative features as in figure 4 except the local maximum that cleanly defines a yield stress and strain is absent, and the stress increases monotonically with strain.

Direct measurement of the segmental (alpha) relaxation time in a polymer glass under active deformation has been recently achieved [57–60]. The alpha time initially decreases strongly with applied stress and strain in a complex and rate-dependent fashion, and then increases in the strain hardening regime [58, 60].

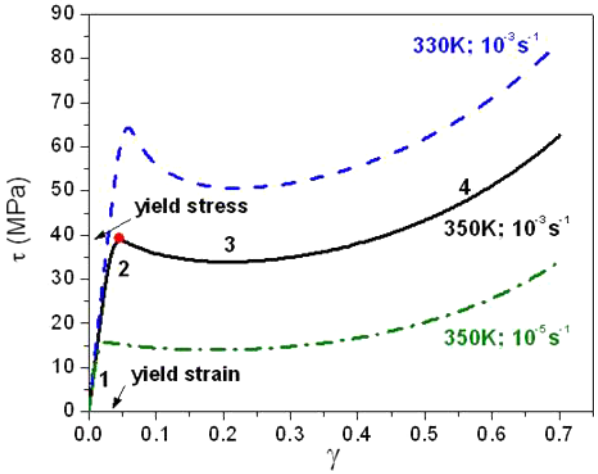

Figure 4. Typical stress–strain curves for a constant strain rate mechanical experiment below T_g. The red dot indicates the yield point and four regimes are marked by numbers. The dashed and dash–dot curves show the effect of temperature and strain rate, respectively. The curves follow from the NLE theory for PMMA glass with rejuvenation included [114], but are presented here as only an illustration of the experimental behavior.

3. Cold polymer liquids

We now discuss recent theories in the equilibrated isotropic liquid state. The primary focus of this section is the mean alpha relaxation time.

3.1. Configurational entropy theories

Modern configurational entropy theories involve major extensions of the Adams–Gibbs picture. Their central concern is the alpha relaxation time, not time correlation functions or mechanical properties. We discuss two approaches: (i) the generic random first order transition (RFOT) theory, and (ii) the polymer-specific lattice cluster entropy theory (LCET), both of which have been reviewed in depth recently [34, 35].

3.1.1. Random first order phase transition theory. The RFOT approach is a mesoscopic entropy crisis theory which employs mode coupling, density functional and spin glass concepts [34]. Vitrification is described analogously to crystallization but in terms of a set of statistically distributed aperiodic structures. The highest relevant temperature is T_A where molecules become transiently caged, which is equivalent to a simplified version of MCT where an aperiodic structure persists forever. Relaxation can occur within finite regions (clusters or 'entropic droplets' of diameter ξ), where particle locations change on a small Lindemann length scale ($\sim 0.1d$). The theory is based on a local free energy landscape where finite barriers separate distinct disordered structures. Rearrangements are entropically favored due to the combinatorial entropy associated with amorphous packing degeneracy, but entail a free energy cost due to a 'mismatch penalty' for accommodating a rearranged particle cluster into an environment composed of localized neighbors.

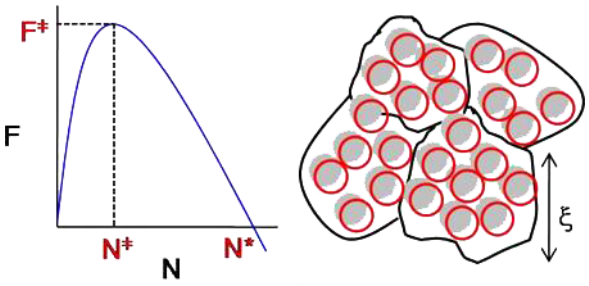

Figure 5. Schematic illustration of the RFOT mosaic picture [34]. Left panel shows the droplet free energy as a function of number of rearranging particles. Right panel indicates the small scale particle rearrangements associated with two aperiodic packings in a domain of diameter ξ. Such a domain model is also relevant to the PFVD and NLE approaches.

The number of rearranging particles at the transition state is determined in the spirit of a nucleation calculation (figure 5) that involves a favorable bulk driving force quantified by the droplet configurational entropy, and an unfavorable interfacial free energy deduced by a combination of density functional, 'fluctuation-induced wetting', and universality of Lindemann parameter arguments. The total free energy as a function of domain radius (R) is

$$F(R) = -\frac{4}{3}\pi T S_c(T) R^3 + 4\pi\gamma_0 \left(\frac{d_0}{R}\right)^{1/2} R^2 \qquad (12)$$

where d_0 is an interparticle spacing, and the second term is the renormalized interfacial free energy which scales more weakly than as surface area. The mean relaxation time is computed as a simple activated process and has the classic VFT form of equation (5) where

$$S_c(T) = \Delta\tilde{C}_p(T)\left(\frac{T - T_K}{T_K}\right) \qquad (13)$$

$$F_B = k_B T D \frac{T_K}{T - T_K} \qquad (14)$$

$$D = \frac{27\pi}{16}\frac{n k_B}{\Delta\tilde{C}_p(T)} \ln^2\left(\frac{\alpha_L R_0^2}{\pi e}\right). \qquad (15)$$

Here, F_B is the barrier, α_L is the square inverse of the Lindemann ratio, and $\Delta\tilde{C}_p(T)$ is the specific heat jump per unit volume at the glass transition. The typical droplet diameter is

$$\xi \propto d_0 \left(\frac{D T_K}{T - T_K}\right)^{2/3} \qquad (16)$$

which differs from the classic AG model. The relaxation time diverges at T_K.

RFOT theory directly relates thermodynamics to slow dynamics. To obtain precise predictions requires the configurational entropy and a definition of 'elementary units' that maps real molecules onto the model. Polymer properties such as monomer shape and backbone persistence length do not enter explicitly, and *a priori* computations of T_A or T_g have not been performed. RFOT does accurately predict dynamic fragility with melting entropy as input [61]. It has been applied to explore the combined effects of temperature and pressure on relaxation for a Lennard-Jones fluid [62]. A largely phenomenological effort has been recently made to combine RFOT theory with a schematic version of MCT to provide a unified description of the crossover and deeply supercooled regimes [63].

Recent analysis [64] suggests the RFOT theory is only one of many possible entropy crisis approaches based on spin glass ideas. Outstanding questions include how to go beyond mean field theory via droplet constructs and how the interfacial free energy scales with droplet radius, issues which can strongly impact the form of the alpha relaxation time.

3.1.2. Lattice cluster entropy theory. The DiMarzio polymer-specific entropy crisis theory [14–16] makes many predictions for the variation of the Kauzmann temperature with molecular weight, chain topology, backbone stiffness, crosslinking and other characteristics based on a mean field lattice model, which are qualitatively similar to the experimentally observed trends for T_g. However, the true meaning of T_K and relevance of the vanishing entropy postulate remains controversial. The LCET [35, 65–68] attempts to surmounts these difficulties by assuming glass formation is driven by a critically small (not zero) configurational entropy computed using the equilibrium lattice cluster theory [69]. The latter includes short range packing correlations due to chain connectivity, monomer shape, and backbone and sidegroup semiflexibility within a united atom framework. The major predictions of this *molecular-level* polymer theory include the temperature dependence of S_c, the relaxation time, and characteristic temperatures.

Polymers are typically modeled as belonging to three classes: FF (flexible backbone and sidegroups), FS (flexible backbone, stiff sidegroups), or SF (stiff backbone, flexible bonds). Chains with stiff backbones or sidegroups have lower configurational entropy density, while flexible sidegroups plastify the polymer. The *monomer* configurational entropy density increases monotonically with temperature, while the *site* configurational entropy density passes through a maximum and decreases at both high and low temperatures (figure 6). This distinction, which rests on the thermal dependence of the density, is key to the formulation of the LCET.

Four characteristic temperatures are introduced based on the site configurational entropy density. The highest is the onset of the glassy regime, T_A, where S_c is a maximum. The glass transition temperature, T_g, is identified with a critical root-mean-square particle displacement estimated via a critical excess free volume, or alternatively as when the relaxation time attains a threshold value. An intermediate crossover temperature, T_c, is the inflection point in the temperature dependence of configurational entropy which separates two regimes of entropy evolution. It is identified with the empirical MCT temperature, a supposition supported by agreement between experimental and calculated estimates of T_c/T_g. Finally, an ideal glass transition temperature, T_0, signals when the configurational entropy *extrapolates* to (not literally equals) zero.

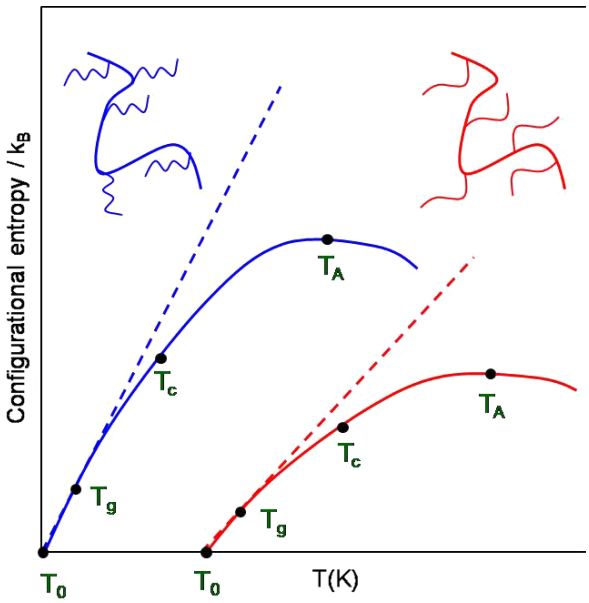

Figure 6. Schematic illustration of the configurational entropy per site predicted by the LCET theory [35] as a function of temperature, with characteristic temperatures marked, for polymers with flexible side chains (blue, left curve) and stiff side chains (red). Dashed curves are the corresponding configurational entropy/mol.

The structural relaxation time is given by the Adams–Gibbs relation, equation (4), where the high-temperature activation energy is related to the empirical MCT temperature via the (nearly) universal crossover relaxation time observed experimentally [41]: $\Delta\mu/k_B \approx (7 \pm 1)T_{MCT}$. A critical power law fit can describe LCET calculations over a range of 60–70 K with a polymer stiffness-dependent critical exponent $\Delta \sim 2.1$–2.8. The temperature dependence of the relaxation time of many polymers can be collapsed onto a universal form via the reduced parameter

$$X = \frac{T_c/T - 1}{T_c/T_g - 1} \tag{17}$$

as seen experimentally for polymer melts and other glass-formers [70].

The characteristic temperatures and fragility grow with molecular weight, saturating for long chains. Glassy behavior is enhanced by increased backbone or sidegroup stiffness due to the larger excess free volume of inflexible bonds. Flexible polymers have larger characteristic temperature ratios (T_c/T_g, etc) corresponding to their lower fragility. Theoretical estimates for the apparent VFT fit parameters compare well with experiment, and the pressure dependence of the relaxation time can be naturally calculated. The experimental chemical structure trends for T_g and fragility discussed in section 2.2 are qualitatively well captured by the theory. The unifying concept that emerges is that local interchain packing controls the fragility to leading order.

3.2. Percolation free volume distribution theory (PFVD)

The free volume model has been extended to include spatial domains and a distribution of relaxation times in conjunction with a physical ansatz that associates the alpha relaxation with percolation of slow domains [36, 71, 72]. Density fluctuations (via liquid compressibility) are the source of spatial heterogeneity with domains distinguished by their density (figure 5). No explicit account is taken of polymer stiffness or monomer shape, which enter implicitly via an equation-of-state and empirical parameters in equation (3) which is viewed as a bare 'monomer' relaxation time.

The PFVD model has been extensively applied to polymer melts [71, 72] using a van der Waals model for equilibrium properties where the key energy scale is set by the cohesive energy density. A 'dynamical' free volume fraction is introduced and defined as

$$\Delta\tilde{\rho} \equiv \frac{\rho_{max} - \rho_{eq}}{\rho_{max}}. \tag{18}$$

Here, ρ_{eq} is the equilibrium bulk density, and ρ_{max} is the $T = 0$ random close packing (RCP) density, but in practice is used as a fit parameter which is significantly smaller. The free volume distribution in a spatial domain of volume V_c is assumed to be determined by spontaneous equilibrium thermal density fluctuations

$$P(\delta\rho) \propto \exp[-(\delta\rho)^2 \kappa_T V_c/2\rho_{eq}^2 T] \tag{19}$$

where $\delta\rho = \rho - \rho_{eq}$ and κ_T is the isothermal compressibility. Bulk relaxation is postulated to be controlled by percolation of slow domains (~10%) corresponding to upwards density fluctuations on the few nm scale, and the observed (mean) alpha relaxation time is determined by the timescale associated with this percolation. This approach differs from the Cohen–Grest percolated-FVM which adopts a binary fluid and solid cell model [73].

Two competing relaxation mechanisms enter the PFVD model. (i) Monomer hopping at fixed local free volume which occurs on a timescale that increases strongly as the local density grows and is the dominant process for self-diffusion

$$\tau_{monomer} = \tau_0 \exp\left(\frac{\theta}{\Delta\tilde{\rho}}\right) \tag{20}$$

where $\theta \sim 1$. Only jumps of the slowest 10% monomers contribute to relaxation. (ii) *Collective* density fluctuation relaxation, which is dominant for monomer relaxation of slow particles, and can be viewed as a type of 'dynamic facilitation' [31] where constraints on a slow monomer are released by diffusion and relaxation of faster neighboring subunits. The collective relaxation time for a domain of N particles is associated with diffusion on the domain scale and is given by [72]:

$$\tau_{life}(N) \sim \tau_0 N^{2/3} \exp\left(\frac{\theta}{\Delta\tilde{\rho} + b\Delta\tilde{\rho}N^{-1/2}}\right) \tag{21}$$

where $b \sim 1$. The relevant number of elementary units, N_c, corresponds to the smallest length scale at which $\tau_{life}(N)$ is equal to, or larger than, the monomer relaxation time. Density fluctuations on smaller scales are irrelevant since they are too short lived. A consequence of the competition between single

particle hops and collective relaxation triggered events is there are two long time cutoffs of the relaxation time distribution associated with the percolation process and a faster subunit 'dynamic melting' process.

The PFVD model has been quantitatively applied to predict how pressure modifies glassy relaxation of flexible polymers with low internal barriers, and good fits to experimental data are obtained [72]. The theory has been generalized and applied to the thin polymer film glass transition problem [74], including a recent variant relevant to polymer nanocomposites [75]. The large and spatially long range confinement effects observed are suggested to be a consequence of mobility percolation.

3.3. Nonlinear Langevin equation theory (NLE)

3.3.1. General formulation. The nonlinear Langevin equation theory (NLE) is a first principles statistical mechanical description of *single* particle motion formulated at the level of molecules and forces [76, 77]. It is built on a locally solid-state view of highly viscous dynamics which employs and extends ideas of MCT and dynamic density functional theory. The approach was initially formulated in a fully microscopic and physically-motivated, but heuristic, manner for spherical particle fluids, and subsequently derived from time-dependent statistical mechanics [78]. The two key approximations are: (i) the dynamical caging constraints experienced by a tagged particle are treated in an average manner via the radial distribution function, $g(r)$, or structure factor, $S(q)$, and (ii) a local equilibrium approximation at the dynamical variable, *not* traditional ensemble-averaged, level is adopted which relates one and two body dynamics and provides a *non*Gaussian closure at the single particle level. The physical idea underlying the latter simplification is that there exists a high degree of dynamical correlation between pairs of particles which preserves local structural correlations in the highly viscous regime [78].

The central premise of NLE theory is that MCT accurately describes the onset of transient localization, but the ideal kinetic glass transition is destroyed and rendered a crossover by an activated barrier hopping process which controls the low-temperature or high volume fraction regime that *smoothly* emerges from the precursor regime. If hopping is ignored, a simple 'naïve' version of MCT (NMCT [76, 79]) for the single particle localization length ($r_{\rm loc}$) is recovered which is quantified by the long time limit of the force–force correlation function on a tagged particle within an amorphous Einstein solid model. The NLE theory does *not* invoke thermodynamic or kinetic divergences at nonzero temperatures or volume fractions below RCP [80]. Its single particle nature implies neglect of a class of dynamical collective density fluctuations (typically called 'feedback' in the MCT language) that are important in the precursor regime [27, 81] and perhaps beyond.

The central object of the theory is a closed, overdamped nonlinear Langevin equation of motion for the instantaneous scalar displacement of a particle from its initial location, $r(t)$, the qualitative form of which resembles Kramers theory [82] or model A:

$$\zeta_{\rm s}\frac{\partial r(t)}{\partial t} = -\frac{\partial F_{\rm eff}[r(t)]}{\partial r(t)} + \delta f(t) \tag{22}$$

where the random force satisfies $\langle \delta f(0)\delta f(t)\rangle = 2k_{\rm B}T\zeta_{\rm s}\delta(t)$, and $\zeta_{\rm s}$ is a short time friction constant. The 'dynamic free energy' is the key object and consists of two contributions

$$\beta F_{\rm eff}(r) = -3\ln(r) - \int \frac{{\rm d}\vec{q}}{(2\pi)^3}\rho C^2(q)S(q)[1+S(q)]^{-1} \times \exp\left\{-\frac{q^2r^2}{6}[1+S^{-1}(q)]\right\} \tag{23}$$

where $\beta \equiv (k_{\rm B}T)^{-1}$, $C(r)$ is the direct correlation function, and $S(q)$ the collective static structure factor. The second term in equation (23) describes interparticle caging forces that favor transient localization. Its non-Debye–Waller part is called the 'vertex' which quantifies the mean square amplitude of dynamical constraints on a length scale $\sim 2\pi/q$ [83]. The NLE theory has been quantitatively applied to fluids of spherical and nonspherical rigid objects [85, 86] in an *ab initio* manner, both analytically using Kramers theory and Green–Kubo formulae [76, 77, 84, 85], and via trajectory simulation solution of equation (22) which allows dynamical nonGaussian effects to be determined [81, 86–88].

3.3.2. Extension to polymer melts. Polymer melts are chemically complex, exhibit nonuniversal short time dynamics, and have connectivity induced local dynamical correlations. For these reasons, the NLE theory analog for polymer melts is more primitive, and is based on a statistical segment description [37, 89, 90]. To a first approximation, the dynamical consequences of chain connectivity beyond the σ scale are ignored corresponding to a 'liquid of segments' description. An analytic 'Gaussian thread' chain model is adopted [91]. At the segment level the sub-nm structural and interaction potential length scales are averaged over, resulting in a site–site direct correlation function $C(q) = C_0$, and collective structure factor $S^{-1}(q) = S_0^{-1} + \frac{1}{12}q^2\sigma^2$, where $S_0 \equiv S(q=0) = \rho k_{\rm B}T\kappa = (-\rho C_0)^{-1}$ is the dimensionless isothermal compressibility which quantifies nanometer and beyond thermal density fluctuations, $\sigma = \sqrt{C_\infty}l$, and $\rho\sigma^3 \sim 0.7$–1.5 is the reduced segmental density. At this lightly coarse grained level, $F_{\rm eff}(r)$ is determined entirely by a single material-specific 'coupling constant'

$$\lambda \equiv \frac{1}{\rho\sigma^3 S_0^{3/2}} \tag{24}$$

which increases with cooling or pressure, and involves only experimentally measurable equilibrium quantities. An example of the dynamic free energy is shown in figure 7.

Minimization of the nonequilibrium free energy with respect to the single segment displacement, or dropping the thermal noise term in equation (22), yields a self-consistent localization equation for the NMCT glass transition which occurs at $\lambda_{\rm c} = 8.32$. Polymer theory and experiment suggest [37] a simple temperature dependence for S_0:

$$S_0^{-1/2} = -A + (B/T) \tag{25}$$

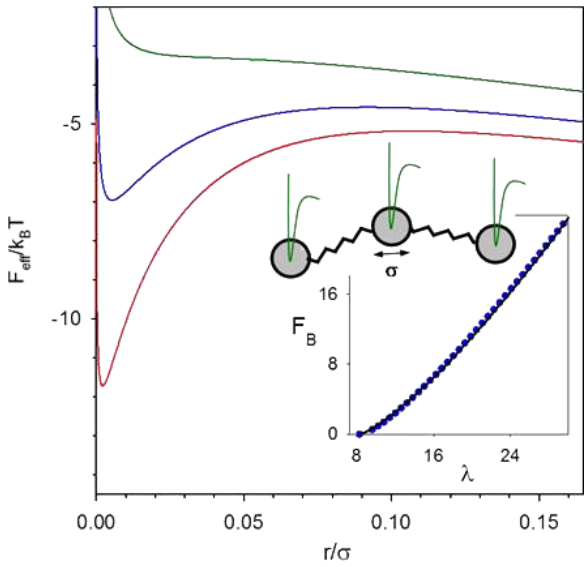

Figure 7. Dynamic free energy as a function of segmental displacement of the NLE theory [37] for polyvinylacetate at coupling constants (from top): $\lambda = 8$ ($T_c/T \sim 0.99$), 12 ($T_c/T \sim 1.11$), 16 ($T_c/T \sim 1.20$). Also schematically shown is a Gaussian chain with each segment experiencing a dynamic confinement potential. Inset: Barrier height (units of k_BT) as a function of the coupling constant with critical power law fit of equation (27).

where $A > 0$ is of order unity, and typically $B \sim 700$–1300 K which correlates with monomer polarity and cohesive energy. Combining equations (24) and (25) gives a first principles prediction for the crossover or ideal MCT temperature

$$T_c = \frac{B}{A + (\lambda_c \rho \sigma^3)^{1/3}}. \tag{26}$$

A priori calculations of T_c yield experimentally reasonable results [37, 89].

In the full NLE theory with thermal noise of equation (22) there is a smooth crossover to the deeply supercooled regime below T_c where collective barriers emerge due to interchain forces. The inset of figure 7 shows the barrier height, F_B, as a function of the coupling constant. Calculations are well described by a critical power law form:

$$\beta F_B \approx c(\lambda - \lambda_c)^{\Delta}, \qquad c \cong 0.4, \quad \Delta \simeq 1.4. \tag{27}$$

Although the barrier height is a universal function of the dimensionless coupling constant, its temperature dependence is material specific.

3.3.3. Alpha relaxation time and shear modulus. Above T_c, dynamics is viewed as an intra-segment-scale Arrhenius process with a relaxation time $\tau_0(T) \equiv \tau_0 \exp(\varepsilon_A k_B T)$, where $\tau_0 \approx 10^{-14\pm1}$ s is a vibrational timescale and ε_A is a local activation energy [37]. Below T_c, the intra-segment dynamics is treated as the fast process that sets the timescale for the alpha relaxation. This motivates a minimalist model that smoothly bridges the normal and supercooled regimes:

$$\tau_\alpha(T) = \tau_0 \exp\left(\frac{\varepsilon_A}{k_B T}\right) \exp\left[\frac{a_c F_B(T)}{k_B T}\right]. \tag{28}$$

Equation (28) ignores a narrow intermediate temperature regime that bridges the Arrhenius and deeply supercooled regimes, and in this sense it does not clearly distinguish between T_A and T_c (but full numerical solution of the NLE does [86–88]). The local activation energy is determined by adopting the recent proposition [41] of a (nearly) universal 'magic relaxation time' at the dynamical crossover given by $\tau_0(T_c) \cong 10^{-7\pm1}$ s; this condition yields: $\varepsilon_A \cong (16.1 \pm 2.5) k_B T_c$ for $\tau_0 \approx 10^{-14}$ s. Alternative 'calibrations', such as a nearly universal relaxation time at T_A of $\sim 10^{-10}$ s, do not change key predictions [89].

In reality, short range equilibrium correlations along the chain due to backbone stiffness are expected to introduce an '*intra*chain cooperativity' of the barrier hopping event. To crudely model this polymeric effect in a non-first-principles manner, a material-specific (but temperature-*independent*) cooperativity parameter, a_c, is introduced resulting in an effective barrier of $a_c F_B$ [37, 90]. Physically, a_c is the number of dynamically correlated segments along the chain, which can be estimated by equating the end-to-end distance of the dynamically cooperative segment ($\sqrt{a_c}\sigma$) to the Kuhn or persistence length thereby yielding $a_c = C_\infty$ or $a_c = (C_\infty + 1)^2/4C_\infty$, respectively; since $C_\infty \approx 4$–10, $a_c \sim 1$–10. The characteristic ratio generally increases with chain length, which implies the intuitive trend of a finite size increase of the cooperativity parameter as chains get longer.

The NLE theory yields sensible predictions for T_g based on the experimentally-relevant criterion $\tau_\alpha(T_g) = 10^x$ s where $x = 2$–4. The breadth of the glassy regime, T_c/T_g, varies over a wide range of ~ 1.1–1.5 depending mainly on chain stiffness via the local cooperativity parameter. The numerically computed relaxation times can be well-fit over many orders of magnitude by commonly-used empirical multi-parameter functions including the VFT and Bassler–Ferry laws, despite the fact the NLE theory has no kinetic singularities at nonzero temperature [89]. An example of the role of chain stiffness on the temperature dependence of the relaxation time is shown in figure 8 for atactic polymethylmethacrylate (PMMA). The dynamic fragility at the glass transition increases from ~ 60 ($T_g = 326$ K) at $a_c = 1$, to ~ 120 ($T_g = 378$ K) at $a_c = 5$, with the latter in good agreement with experiment [46].

The dynamic fragility depends on chemical variables primarily through $S_0(T)$ and chain stiffness via a_c. Since the equation-of-state properties of most polymers are rather similar, the origin of the large range of dynamic fragilities ($m \sim 45$–180) observed experimentally is predicted to be primarily a consequence of variable backbone stiffness. A statistical correlation has been shown to apply for many polymers [90]:

$$m \approx 16 + 40.6 a_c^{0.56}. \tag{29}$$

Because the characteristic ratio (a_c) generally decreases as chains get shorter, the dynamic fragility decreases as N gets smaller, as often observed [48, 49]. The theory also suggests the long chain limit of fragility is controlled by saturation of the characteristic ratio ($C_N \to C_\infty$) and attainment of full Gaussian statistics.

A universal form for the temperature dependence of the scaled alpha relaxation time in the deeply supercooled regime

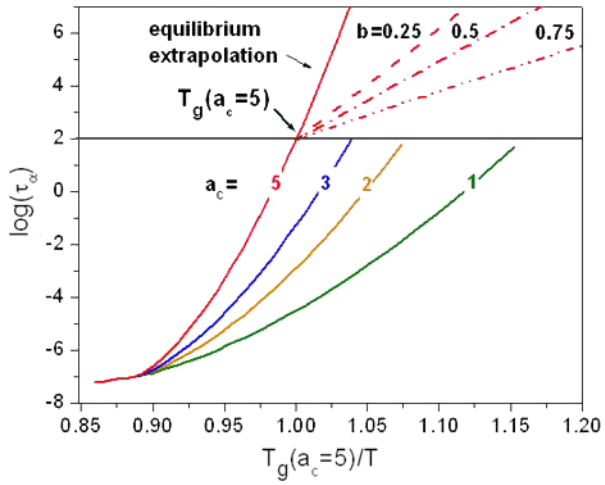

Figure 8. Relaxation time as a function of normalized (by T_g for $a_c = 5$) inverse temperature for PMMA. Above T_g results are shown for several values of the cooperativity parameter. The below T_g results are under quenched glass conditions for $a_c = 5$ for several values of the frozen-in density fluctuation amplitude parameter, b; the uppermost curve is the equilibrium extrapolation.

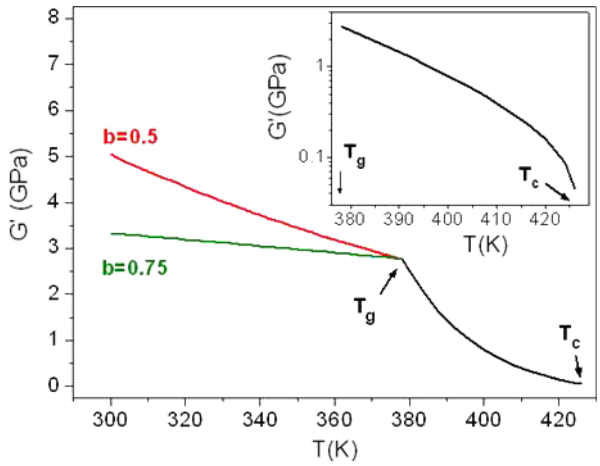

Figure 9. Elastic shear modulus for PMMA ($a_c = 5$) as a function of temperature. Below T_g corresponds to the quenched glass for two values of the frozen-in density fluctuation parameter. Inset: log–linear plot in the deeply supercooled melt regime ($T_g < T < T_c$).

is predicted [37, 89]:

$$lg\left[\tau_\alpha(T)/\tau_\alpha(T_c)\right] = cX^\nu \tag{30}$$

where X quantifies the distance from the dynamic crossover as defined in equation (17), the exponent $\nu \cong 1.4 \pm 0.1$ depends weakly on the dynamic crossover time and temperature range analyzed, and c is a constant. Equation (30) corresponds to a non-analytic, supra-Arrhenius temperature dependence that transcends *all* material details of the theory (segmental density, compressibility parameters A and B, cooperativity parameter, crossover relaxation time, etc). Its basic form, including the magnitude of effective exponent, is in accord with experiments [70]. A corollary is the breadth of the deeply supercooled regime controls fragility as: $m \cong b/[1 - (T_g/T_c)]$, where $b \approx 14 \pm 2$ for $\tau_\alpha(T_c) = 10^{-7\pm1}$ s and $\tau_\alpha(T_g) = 100$ s. The consequences of elevated pressure have been tentatively investigated [90]: equation (30) continues to hold, T_c/T_g decreases with pressure, and hence the fragility increases, trends in agreement with most, but not all, polymer experiments.

Since the NLE theory is formulated at the level of forces and particle positions, mechanical properties such as the glassy elastic shear modulus G' due to *inter*chain stresses can be calculated using the standard Green–Kubo formula [46, 92]; an example for PMMA is shown in figure 9. The dimensionless modulus $G'k_BT\sigma^{-3} \approx 1$ at the dynamic crossover temperature, and is roughly equal to the Rouse shear modulus due to chain conformational entropy [46]. This result provides a zeroth order understanding of why $T_{ll} \sim T_c$ signals the onset of non-entropic elasticity in cold polymer liquids [50]. Below T_c, the modulus increases exponentially, $G'k_BT\sigma^{-3} \sim \exp(aT_c/T)$ where $a \sim 12$. At T_g, the dimensionless modulus is ∼60–70, which corresponds to ∼1–3 GPa, the correct experimental magnitude and a common mechanical definition of a glass [90].

The mapping of a real polymer chain onto the coarse grained Gaussian segment level, and its implications for the collective structure factor, has been discussed [92]. The simplification $C(q) \sim C(q = 0)$ applies for inverse wavevectors larger than of order a nanometer. The atomistic level $S(q)$ of polymer melts determined from experiment, simulation and theory do have the generic form of being nearly constant beyond nm (segmental) length scales. The sensibility of the adopted space–time coarse graining approach was analytically established by demonstrating the wavevector dependence of the vertex in equation (23) is identical at the segment and more atomistic levels. This point was demonstrated numerically by showing good agreement between the vertices of the Gaussian thread and freely jointed chain (FJC) models [92]. In contrast to the Gaussian thread model, a dense melt of FJC polymers is characterized by a nonzero monomer diameter, local chain persistence, short range oscillatory interchain order, and a wide angle cage peak in $S(q)$.

4. Dynamic heterogeneity effects

Dynamic heterogeneity (DH) and cooperativity, two distinct concepts that are not definable at the same level of precision, are important features of deeply supercooled dynamics [93, 94]. Whether DH is a 'side show' [93] to a dynamical mean field theory of alpha relaxation, or the dominant physics of glassy dynamics, continues to be debated. At zeroth order, models separate into two categories depending on whether DH is viewed as a dynamically emergent phenomenon or as a consequence of a (quasi) static domain picture where thermodynamically controlled local fluctuations lead to a distribution of barriers and relaxation times. The theories discussed in the present article largely fall in the latter category, and figure 5 is relevant.

4.1. Configurational entropy theories

Dynamical heterogeneity in RFOT theory is due to the mosaic droplet structure with domains treated as effectively static and non-interacting to leading order [34, 95]. The free energy barrier for rearrangement varies between droplets due to equilibrium spatial fluctuations of the configurational entropy. The characteristic length scale of equation (16), or number of cooperatively rearranging elementary units, grows strongly with decreasing temperature. Stretched exponential relaxation approximately follows as a consequence of a Gaussian barrier height distribution with a variance proportional to the configurational entropy fluctuation squared. The corresponding stretching exponent is [95]:

$$\beta_{\rm K} \simeq [1 + (\bar{F}_{\rm B}/2\sqrt{D})^2]^{-1/2} \tag{31}$$

where the fragility parameter D is given by equation (15), and $\beta_{\rm K}$ decreases significantly with temperature. RFOT predicts a direct relation between a larger D and a smaller stretching exponent, which has statistical support from experiments [43]. A static domain model does not allow high barriers to be destroyed via the relaxation of surrounding low-barrier regions. The simplest incorporation of such a 'facilitation' effect [31, 32] is the high-barrier portion of the distribution is replaced by a delta function at its most probable value. RFOT has recently been semi-empirically combined with a simple version of MCT to address the time dependence of the entropic droplet barrier distribution [63].

RFOT predicts translation–rotation decoupling [96]. The translational diffusion constant is determined by a static average over the distribution of local inverse relaxation times which becomes increasingly larger compared to the inverse of the mean relaxation time as the distribution broadens. Decoupling grows with cooling, and increases in magnitude at $T_{\rm g}$ as the liquid becomes more fragile, trends consistent with experiment.

In the explicitly polymeric LCET approach the length scale associated with dynamical heterogeneity is the Adams–Gibbs cooperatively rearranging region comprised of $z^* \equiv s_{\rm c}^*/s_{\rm c}$ elementary units. The CRR grows with decreasing temperature from $z^* = 1$ at $T_{\rm A}$, to $z^* \sim 2$ at $T_{\rm c}$, to $z^* \sim 4$–5 at $T_{\rm g}$. Motivated by the observation of transient clusters of mobile particles in glassy colloidal suspensions and simulation models of glassy fluids, the theory considers DH in the context of equilibrium polymerization [35]. The idea is that the temperature evolution of dynamically correlated regions is a clustering process similar to the activated formation of chains from monomers. In the normal fluid regime, as at the beginning of a polymerization reaction, there is no clustering. During the reaction (supercooled liquid regime) the system is composed of chains or strings with a distribution of lengths, corresponding to a distribution of dynamic clusters. Saturation of the polymerization reaction corresponds to the glass transition at which the system falls out of equilibrium.

4.2. PFVD theory

Dynamic heterogeneity arises from the distribution of relaxation times due to variable density domains. The PFVD model predicts the domain size, or number of cooperatively rearranging units ($N_{\rm c}$), monotonically increases upon cooling. Numerical applications to polymers yield $N_{\rm c} \sim 100$–700 at $T_{\rm g}$, but these estimates are sensitive to unknown prefactors and the ambiguity of what an 'elementary unit' is for polymers [74].

The theory also predicts temperature-dependent relaxation–diffusion decoupling based on the postulate that only the slowest 10% of moving elements contribute to relaxation, which heavily weights the long time part of the distribution. In contrast, mass transport is dominated by the fastest relevant timescale controlled by a short time cutoff, and the diffusion constant scales as the average of the inverse relaxation time. Applications to probe motion in cold polymer melts have been carried out and agreement with experiment demonstrated based on multiple fitting parameters [74].

4.3. NLE theory

There are two sources of heterogeneity in the NLE theory, which have been thoroughly worked out for hard sphere fluids and colloidal suspensions [86–88, 97]. The essence of the results applies to polymer melts, although this has not been fully documented in the literature.

The first DH mechanism arises even when the dynamic free energy is uniquely defined (*spatial homogeneity* of caging constraints). The reason is activated hopping is driven by thermal noise fluctuations, resulting in a distribution of hopping times corresponding to purely *temporal* DH. Consequences include weakly nonexponential relaxation, diffusion–relaxation decoupling, exponential tails in the van Hove function, growing dynamical correlation lengths, and large nonGaussian parameters [86–88]. For a generic time correlation function, the Poissonian hopping time distribution that applies for high enough barriers results in nonexponential relaxation [86]:

$$C(t) = \int_0^\infty {\rm d}\tau_\alpha \frac{\tau_\alpha}{\bar{\tau}_\alpha^2} {\rm e}^{-\tau_\alpha/\bar{\tau}_\alpha}\, {\rm e}^{-t/\tau_\alpha} = K_2(2\sqrt{t/\bar{\tau}_\alpha}/3) \tag{32}$$

where K_2 is the incomplete Bessel function of order two. At long times this is a stretched exponential with a temperature or volume fraction *independent* exponent of $\beta_{\rm K} = 0.5$.

A second origin of DH is based on the (quasi) static domain model with density fluctuations and equation (19). The cooperativity domain diameter, ξ, is qualitatively identified with the density fluctuation correlation length [97], $\xi \sim 2(d + \xi_\rho) \sim$ 3–6 nm. A crucial feature is ξ is *independent* of temperature or volume fraction to leading order, which seems consistent with both potential energy landscape analyses [26] and attempts to understand segmental friction factors in binary polymer blends [98], but is *very different* from the AG-like picture that underlies the configurational entropy theories.

For hard sphere fluids the consequences of the Gaussian barrier distribution model have been worked out in detail [97]. The mean relaxation time is only modestly enhanced by fluctuations. Fractional Stokes–Einstein (FSE) decoupling of relaxation and diffusion is predicted (at the segmental scale for polymers) corresponding to

$$D \propto \langle \tau_\alpha^{-1} \rangle \propto \langle \tau_\alpha \rangle^{-\varepsilon} \qquad \varepsilon \equiv \frac{1-\delta}{1+\delta}, \qquad \delta \equiv \frac{\sigma_F^2}{2\bar{F}_{\rm B}} \tag{33}$$

where δ is the dimensionless ratio of the barrier fluctuation variance to the most probable barrier height. Nonexponential relaxation approximately emerges with a stretching exponent that decreases as the degree of decoupling grows:

$$\beta_{\rm K} \simeq \frac{1}{\sqrt{1+\ln(r)}}, \qquad r \equiv \langle \tau_\alpha^{-1} \rangle \langle \tau_\alpha \rangle \tag{34}$$

where the decoupling factor, r, increases with cooling or volume fraction.

Perhaps the most interesting consequence of this domain model is for the decoupling of segmental and chain end-to-end relaxation and TTS failure discussed in section 2.2. The idea is that on the macromolecular scale, space–time heterogeneous dynamics is averaged over, while on the nm scale relevant to the segmental alpha process it is not. A testable prediction has been made for the decoupling exponent in equation (11) [54]:

$$\frac{1}{\varepsilon} \simeq 1 + \frac{\delta^{-1}}{[(m-16)/40.6]^{1/0.56}} \tag{35}$$

where equation (29) has been used. This result is in excellent agreement with experiments for $\delta \sim 0.1$–0.2, reasonable values based on *a priori* estimates, and provides a possible mechanism for the observed strong coupling between segmental fragility and the FSE exponent [54]. This theoretical perspective also provides a basis for the experimental observation that the dynamic fragilities of the macromolecular scale relaxation process are both smaller and much less variable than their segmental relaxation analogs [49, 54]. However, this explanation of TTS failure remains tentative in the sense that full consistency of the physical picture with other DH signatures remains to be demonstrated.

How the two DH mechanisms discussed above might be combined to produce a unified description within the NLE framework remains an open question. We note a recent empirical modeling attempt to describe temperature-dependent stretched exponential relaxation in a variety of cold polymer melts that combines an ad hoc VFT-based static domain model with intrinsic dynamical fluctuation effects [45].

5. Bulk anisotropic polymer materials

Macroscopic anisotropy is a distinguishing feature of polymeric fluids. The simplest class is spatially homogeneous liquid crystals and deformed rubber networks, both characterized by structural anisotropy at the segmental and macromolecular levels (figure 3). Conformational anisotropy induces anisotropic *inter*chain correlations and density fluctuations. To understand the latter requires theories that link anisotropic structure and dynamics. Recent progress in this direction has occurred based on the polymer NMCT and NLE approaches [99], which are rendered predictive based on the anisotropic polymer reference interaction site model (PRISM) integral equation theory [100, 101]. How the *scalar* $T_{\rm c}$ or $T_{\rm g}$ change requires understanding the subtle question of how anisotropic dynamical constraints are 'averaged over'.

Polymer NMCT predictions for the dynamical crossover temperature have been worked out based on two coupled self-consistent equations for the localization lengths ($r_{{\rm loc},\parallel} \neq r_{{\rm loc},\perp}$) which involve different force–force correlations with 'vertices' that reflect the spatial anisotropy [99]. The latter enters the dynamical calculation in two distinct manners: (i) the critical value of the coupling constant, $\lambda_{\rm c}$ of equation (24), and (ii) the dimensionless compressibility ($S_0 = -1/\rho C_0$ in the long chain limit), which both depend on the order parameter and nature of the anisotropy.

5.1. Liquid crystals and oriented melts

In a nematic or discotic polymer liquid crystal, or if a polymer melt is subjected to an external electric or magnetic field, segmental bond vectors undergo alignment with distinct parallel and perpendicular components relative to a director, $\sigma_\parallel \neq \sigma_\perp \neq \sigma_0$ (where σ_0 is the isotropic melt value), quantified by the order parameter:

$$\tau_{\rm or} = \left\langle \frac{3\cos^2(\theta) - 1}{2} \right\rangle. \tag{36}$$

Here θ is the angle between a segmental bond vector and the director, and the order parameter is positive in nematics ($0 < \tau_{\rm or} < 1$) and negative in discotics ($-0.5 < \tau_{\rm or} < 0$) (figure 3). The macromolecular length scale, $R_{\rm ee}$, is also anisotropic but its consequences can be neglected to leading order [99]. Chain conformation is described as a *directed* Gaussian random walk with different step lengths: $\sigma_\parallel = \sigma_0(1-\tau_{\rm or})$ and $\sigma_\perp = \sigma_0\sqrt{1+2\tau_{\rm or}}$, respectively [100]. For excluded volume interactions, PRISM theory predicts chain orientation results in an *increase* of the amplitude of collective density fluctuations. The reason is that alignment reduces the degree of chain interpenetration and hence repulsive interchain contacts, in analogy with the Onsager theory of liquid crystallinity. This results in a *decreased* driving force for glass formation. On the other hand, the anisotropic static structure factors that enter NMCT reduce $\lambda_{\rm c}$ which *favors* glass formation. Numerical studies [99] find the former effect is dominant, resulting in a *reduction* of $T_{\rm c}$ with alignment which grows as roughly a parabolic function of $\tau_{\rm or}$. For typical material parameters, normalized reductions are $(T_{\rm c}(\tau_{\rm or}) - T_{\rm c}(0))/T_{\rm c}(0) \sim 5\%$ for $\tau_{\rm or} \sim \pm 0.2$, and $\sim$15% (23%) for 0.4($-$0.4). Definitive experiments or simulations to test this prediction remain to be performed.

5.2. Strained rubber networks

Anisotropic PRISM and NMCT theories have been developed for crosslinked rubbers [99, 101]. The network is treated as a liquid on length scales smaller than the mean distance between junctions, and N is identified with the network strand length, N_x. A volume conserving uniaxial deformation modifies the end-to-end vectors affinely:

$$R_{{\rm ee},\parallel} = \lambda_{\rm d} R_{{\rm ee},0}, \qquad R_{{\rm ee},\perp} = \lambda_{\rm d}^{-1/2} R_{{\rm ee},0} \tag{37}$$

where $\lambda_{\rm d}$ is the macroscopic deformation ratio (figure 3). Strain introduces tiny segmental orientation, but its consequences on dynamics is very small [99].

PRISM theory predicts strain (compression or extension) monotonically *reduces* the amplitude of long wavelength

density fluctuations (S_0), and more so as segmental density increases or N_x decreases. On the other hand, the critical value of the NMCT coupling constant, λ_c, is almost unchanged even at large deformations. Hence, the effect of deformation on T_c is dominated by bulk modulus hardening (smaller S_0). This results in the *opposite* dynamical behavior of that found for liquid crystals: an *increase* of T_c which grows nonlinearly with the amplitude of deformation $|\lambda_d - 1|$ in a manner that is not symmetrical for tension and compression. For typical flexible chain networks the effect is modest; for example, at $\lambda_d \sim 4$, T_c increases by 5–6% if $N_x \sim 100$–200. Overall, the predicted trends seem consistent with experiment although much more precise and systematic measurements and simulations are needed to draw quantitative conclusions.

6. Nonequilibrium relaxation and physical ageing

Below T_g, freshly quenched samples generally exhibit an Arrhenius alpha relaxation time. As waiting time increases, glass structure evolves towards equilibrium, and thermodynamic, relaxation and mechanical properties become time dependent. Simulations of glassy polymers find the consequences of physical ageing for macroscopic properties are consistent with activated dynamics on the local segmental scale [23].

6.1. Configurational entropy theories

In RFOT theory the initial quenched glass is at ambient temperature for vibrational motions and the fictive temperature ($T_f = T_g$) at the configurational level [102]. In each domain only two states are relevant: quenched or equilibrated with relatively shorter or longer relaxation times, respectively. A macroscopic sample evolves (quasi) continuously due to many small discontinuous changes of the fictive temperature which are driven by both configurational entropy and the energy difference between aperiodic packing states. The alpha relaxation time in the quenched glass gradually transitions to an Arrhenius form with the apparent activation energy decreasing with cooling until saturation at a temperature which depends mainly on T_K/T_g. The specific form can be expressed in the Narayanaswamy–Moynihan–Tool [17] framework as:

$$\tau_\alpha = \tau_0 \exp\left[\chi_{NMT}\frac{\Delta E^*}{k_B T} + (1-\chi_{NMT})\frac{\Delta E^*}{k_B T_g}\right] \qquad (38)$$

where ΔE^* is the equilibrated activation energy at T_g, and the temperature-dependent 'nonlinearity parameter' $0 \leqslant \chi_{NMT} \leqslant 1$. As opposed to phenomenological theories, the nonlinearity parameter can be calculated from the droplet surface tension, heat capacity jump, configurational entropy, T_g and T_K. RFOT then predicts a direct connection between the nonlinearity parameter and dynamic fragility: $m \sim 19/\chi_{NMT}$, which agrees rather well with data for many polymer glasses [103]. The KWW stretching exponent is predicted to decrease with cooling below T_g. Currently, the RFOT theory has not made predictions for the temporal ageing of the alpha relaxation time or other properties.

The lattice cluster entropy theory has been combined with a polymerization (string) view of dynamic heterogeneity [35]. When the excitation chain polymerization saturates, the entropy becomes constant. This is a distinctive mechanism for the crossover of the alpha relaxation time to an Arrhenius form at low temperatures. A melt supercooled more slowly has fewer and larger clusters, and reaches the ageing regime at a lower temperature. This trend is in analogy with the fact that polymerization occurs with a higher activation barrier in order to form fewer total chains.

6.2. Percolated free volume distribution model

The PFVD model describes ageing based on the nonequilibrium evolution of the domain density probability distribution function, $p(\rho)$ [103]. A thermodynamic force $(d/dp)\ln(p/p_{eq})$ is assumed to drive the system towards equilibrium. Based on master equation and Onsager regression type of ideas, a Fokker–Planck equation is proposed:

$$\frac{\partial p}{\partial t} = \frac{\partial}{\partial \rho}\left[\gamma(\rho)p_{eq}(\rho)\frac{\partial}{\partial \rho}\left(\frac{p}{p_{eq}}\right)\right] \qquad (39)$$

where $\gamma(\rho)$ is a diffusion constant in density space which depends on the entire distribution. This diffusion constant is related to the rate of single particle relaxation and collective density fluctuation lifetime within the percolation model framework.

The relaxation time distribution function shifts towards longer times and undergoes complex shape changes with waiting time. Apparent power law ageing of the alpha relaxation time and logarithmic variation of volume are predicted at intermediate ageing times for polymer glasses [103]. However, little change of the apparent exponent with temperature occurs in the shallow quench regime. High asymmetry between up and down temperature jump ageing experiments is predicted due to different time evolutions of the density distribution and dynamic coupling between fast and slow domains (facilitation). The Kovacs memory effect [104] has been studied corresponding to the observation that the time evolution of the glass when it is heated depends on its history and initial nonequilibrium state. The ability of the theory to describe this phenomenon is intimately related to the distribution of relaxation times and domain picture.

6.3. NLE theory

Extension of the NLE theory to treat the alpha relaxation process below T_g is based on the assumption that the dimensionless density fluctuation amplitude, S_0, continues to be the relevant slow variable and caging constraints are quantified by its nonequilibrium value [47, 105]. From a landscape perspective, the compressibility has two contributions: vibrational motions (intrabasin) and larger scale structural rearrangements (interbasin) [106]. Below T_g the second process is effectively turned off after a rapid quench, resulting in an abrupt change in the temperature dependence of S_0. The latter has been extensively studied for polymer

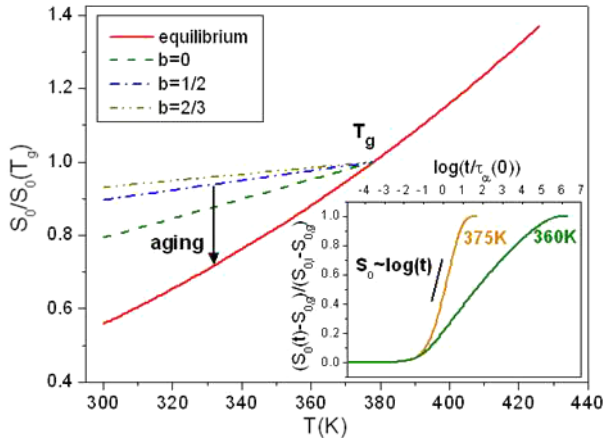

Figure 10. Normalized dimensionless density fluctuation amplitude as a function of temperature for PMMA under quenched conditions and full equilibration. Inset: ageing of $S_0(t)$ in a normalized format per equation (41) after a rapid quench to the indicated temperature.

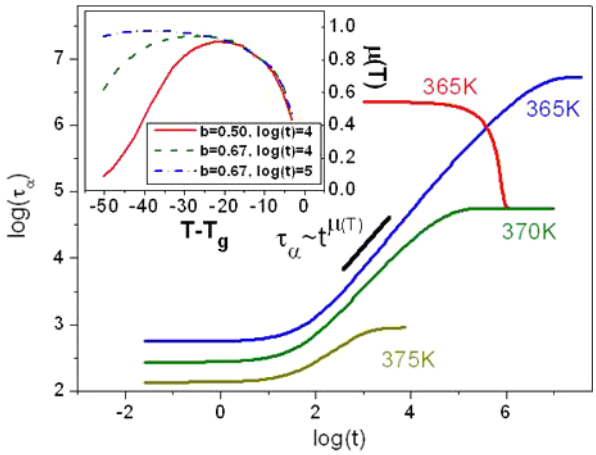

Figure 11. Log–log plot of relaxation time ageing at three quench (down jump) temperatures for PMMA glass ($T_g = 378$ K, $b = 2/3$). One result for an up jump experiment from an equilibrated state at 365–370 K is shown in red. Inset: apparent ageing exponent evaluated at the indicated time after the quench as a function of degree of undercooling.

glasses using small angle scattering[5]. The generic behavior found is: (a) sufficiently far below T_g, $S_0 \propto T$ as in a vibrating harmonic solid; (b) S_0 saturates at a nonzero value at very low temperature due to a frozen-in component of density fluctuations, which can be quantified as $S_0(T \to 0) \equiv bS_0(T_g)$ where $b \sim 0.4$–0.75. This motivates a minimalist, one parameter form for the dimensionless density fluctuations in the *quenched* glass [46]:

$$S_0(T) = bS_0(T_g) + \frac{T}{T_g}(1-b)S_0(T_g). \tag{40}$$

A numerical example for PMMA is shown in figure 10.

The elastic modulus and relaxation time of a freshly quenched (non-ageing) glass have been studied [46]. Figure 9 shows that below T_g the thermal dependence of the shear modulus is nearly linear as observed experimentally. Figure 8 demonstrates there is a crossover of the alpha time to an effectively Arrhenius form below T_g with an apparent activation energy that depends on the frozen density fluctuation amplitude. The ratio of activation energies across T_g, $R \equiv E_A^+/E_A^-$, varies from ∼2–6 as b increases, broadly consistent with experiments[6]. The Arrhenius behavior is a consequence of the nonequilibrium, solid-like nature of density fluctuations in a freshly quenched glass.

To describe physical ageing, a first order kinetic model [105] is proposed for the dynamic order parameter, $S_0(t)$, which evolves from its nonequilibrium quenched value ($t = 0$) given by equation (40) to the smaller equilibrium value, $S_{0,l}$:

$$\frac{\mathrm{d}S_0(t)}{\mathrm{d}t} = -\frac{S_0(t) - S_{0,l}}{\tau_\alpha(t)}. \tag{41}$$

The physical idea is the rate of change at an ageing time t is linearly proportional to how far the system is from equilibrium, and equilibration proceeds via activated barrier hopping which is self-consistently determined by $S_0(t)$ via equations (24), (27) and (28). Equation (41) is devoid of adjustable parameters. Its solution can be written in a normalized time integral form

$$\frac{S_0(t) - S_{0,l}}{S_0(0) - S_{0,l}} = \exp\left\{-\int_0^t [\mathrm{d}t'/\tau_\alpha(t')]\right\}. \tag{42}$$

The inset of figure 10 shows the ageing of S_0 in a normalized format. The time evolution is logarithmic at intermediate times, with a slope that decreases with cooling. Analogous calculations for the shear modulus and cohesive energy density have been performed with similar logarithmic behavior albeit with property-dependent effective slopes [92].

The sigmoidal time evolution of the alpha time for various cooling depths is shown in figure 11. The equilibration time (plateau) increases extremely rapidly with cooling, and is roughly equal to the relaxation time of the final equilibrium state. A good power law behavior, $\tau_\alpha(t) \propto t^\mu$, occurs at intermediate times where the ageing exponent depends strongly on temperature initially, then slowly approaches unity from below, and varies weakly with the frozen density fluctuation amplitude parameter. The exponent μ is determined assuming all timescales are accessible. At sufficiently low temperature, experiments often find a material-specific sharp downturn of the apparent ageing exponent [2]. This nonuniversal behavior has been suggested to originate from the limited time window that experiment can access, i.e. the power law intermediate regime lies beyond the observable timescale [105]. Model calculations in the inset of figure 11 illustrate this point, and the onset of the downturn and the breadth of the plateau are sensitive to the observation timescale. Overall, the theoretical predictions for $\mu(T)$ agree well with measurements on several polymers [92, 105].[7]

[5] See [46] for a detailed summary of experimental measurements of the amplitude of long wavelength density fluctuations in polymer glasses.

[6] See [46] for a detailed summary of the different measurements of apparent activation energy changes of polymer melts across the glass transition.

[7] See [92] and [105] for a description of the ageing experiments that determined the apparent exponent against which the theory has been compared.

The fictive temperature concept has been discussed and its temporal evolution calculated [92]. A strongly asymmetric ageing response for up and down temperature jump experiments is also predicted, as illustrated in figure 11. Dynamic heterogeneity has been empirically investigated by introducing a stretched exponential form into the evolution equation for $S_0(t)$. The apparent ageing exponent is smaller if $\beta_K < 1$, but its temperature dependence is only weakly affected. As presently formulated, the NLE theory does not address the classic Kovacs memory effect.

7. Nonlinear mechanical response in glasses

The nonlinear mechanical behavior of polymer glasses is extremely rich. At present, it appears that the only predictive theory at the segmental level is the NLE barrier hopping approach, which is the subject of this section.

7.1. Effect of stress on relaxation and elasticity

The NLE theory of stress-induced acceleration of segmental relaxation builds on the analogous approach originally developed for colloidal glasses [107]. An applied stress (τ) induces a constant external force on a tagged segment in equation (22) given by: $f = c\sigma^2\tau$, where c is of order unity. The coupling constant, λ, is taken to be unmodified by deformation, i.e. stress does not change glass density nor density fluctuation amplitude. The fast relaxation process $\tau_0(T)$ is assumed to be deformation independent. These simplifications appear to be good first approximations [21, 108]. Moreover, simulations find segmental dynamics is accelerated in an isotropic manner, and there exists a tight coupling between local dynamics and mechanical response [23, 109, 110].

In contrast to the Eyring model [18], stress enters at a microscopic *dynamic variable* level. This idea is equivalent to modeling deformation as a mechanical work type of contribution to $F_{\rm eff}(r)$ which depends on the *instantaneous* segment displacement. A key consequence is stress reduces the barrier for hopping and accelerates relaxation (figure 12) [21], and can mechanically drive a glass-to-liquid transition in a manner qualitatively consistent with landscape simulation studies [111, 112]. The inset of figure 12 shows deformation destroys the barrier at an 'absolute yield stress', $\tau_{\rm abs}$. The shear modulus is also reduced with applied stress due to a growing localization length [21].

7.2. Constitutive equation and yielding

A constitutive equation has been constructed in the Maxwell model spirit that can treat any mechanical deformation (oscillatory shear, step strain, creep, and constant strain rate), and which requires as input only the elastic modulus and mean alpha time from the NLE theory [108]. Here the ideas are explained in the context of elongation and compression experiments and Young's modulus $E(t) \simeq 2.8G(t)$. The

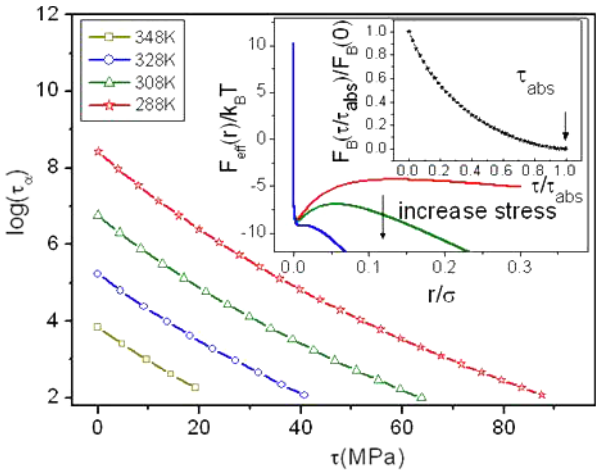

Figure 12. Log–linear plot of stress-induced reduction of the alpha relaxation time of PMMA ($T_g = 378$ K, $b = 2/3$). Inset: dynamic free energy as a function of reduced segmental displacement under stress at $T_g - T = 30$ K; its inset shows a doubly normalized plot of the barrier as a function of applied stress which is nearly temperature independent.

starting point is the Boltzmann superposition principle:

$$\tau(t) = \int_0^t E(t-t')\dot{\gamma}(t')\,\mathrm{d}t' \tag{43}$$

where $\dot{\gamma}(t)$ is a time-dependent strain rate. Equation (43) is adopted as a plausible ansatz by introducing a deformation-dependent modulus that obeys a first order kinetic equation:

$$\frac{\mathrm{d}E(t;\tau(t))}{\mathrm{d}t} = -\frac{E(t;\tau(t))}{\tau_\alpha(\tau(t))}$$
$$E(t-t') = E'(\tau(t'))\exp\left(-\int_{t'}^t \mathrm{d}t''\tau_\alpha^{-1}[\tau(t'')]\right). \tag{44}$$

This is of the classic 'effective time' form, and implies:

$$\tau(t) = \int_0^t \mathrm{d}t' E'(\tau(t'))\exp\left\{-\int_{t'}^t \mathrm{d}t''\tau_\alpha^{-1}[\tau(t'')]\right\}\dot{\gamma}(t'). \tag{45}$$

Equation (45), plus the stressed versions of equation (28) and the Green–Kubo formula for the modulus, comprise a self-consistent, nonlinear description of mechanical response, elasticity and relaxation [108]. A 'granular-like' limit of interest is $\dot{\gamma}\tau_\alpha \to \infty$ corresponding to no thermally-induced activated hopping on the experimental timescale.

For a constant rate experiment the strain $\gamma \equiv \dot{\gamma}t$, and the stress–strain relation is

$$\tau(\gamma) = \int_0^\gamma \mathrm{d}\gamma' E'(\gamma')\exp\left\{-\int_{\gamma'}^\gamma \mathrm{d}\gamma''\frac{1}{\dot{\gamma}\tau_\alpha[\tau(\gamma'')]}\right\}. \tag{46}$$

Plastic flow corresponds to $\mathrm{d}\tau/\mathrm{d}\gamma = 0$, which determines the dynamic yield stress as

$$\tau_y = \dot{\gamma}(E'(\tau_y)\tau_\alpha(\tau_y)). \tag{47}$$

If the product of the strain rate and relaxation time *at dynamic yielding*, $(\dot{\gamma}\tau_\alpha)_y$, is much less than unity, then the post-yield material is locally equilibrated on the segmental scale.

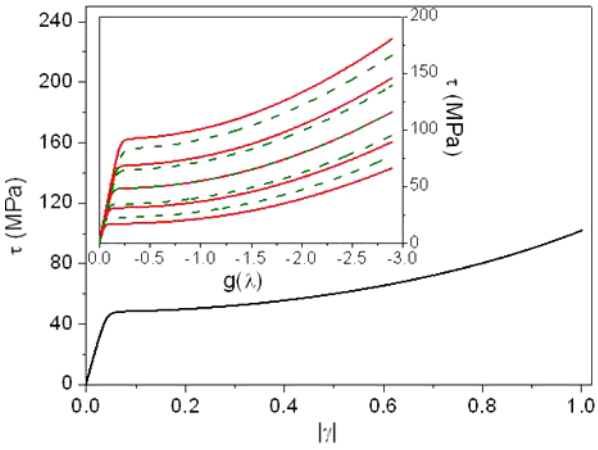

Figure 13. Stress–strain curve under compression for PMMA glass at a strain rate of 0.001 s^{-1} and $T = T_g - 50$ K. Inset: stress–strain curves as a function of the rubber elasticity strain measure $g(\lambda) = \lambda^2 - \lambda^{-1}$ for (solid) strain rate of 0.001 s^{-1} and $T_g - T$ (top to bottom) of 90, 70, 50, 30 and 10 K, and (dashed) at fixed $T = T_g - 50$ K for strain rates (top to bottom) of 10^{-1}, 10^{-2}, 10^{-3}, 10^{-4}, 10^{-5} s^{-1}.

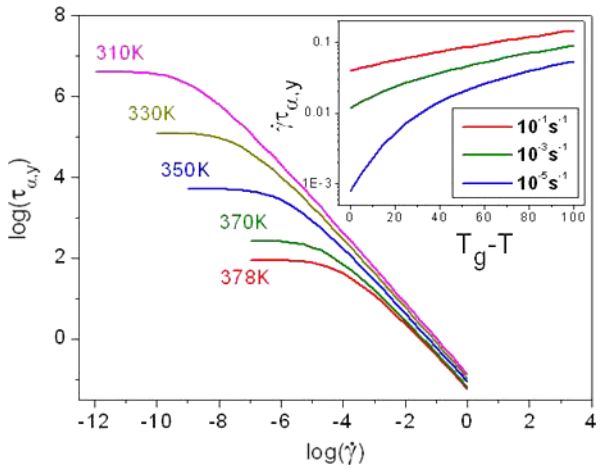

Figure 14. Log–log plot of the relaxation time of PMMA glass ($T_g = 378$ K) in the yield plateau regime (in the absence of strain hardening) as a function of strain rate. Inset: product of the relaxation time at yield and the corresponding strain rate as a function of cooling depth at various rates.

Stress–strain curves for PMMA ('plexiglass') are shown in figure 13. All the regimes observed experimentally (see figure 4) are captured with the exception of the local maximum at the yield point. The yield strains and plateau yield stresses are well predicted as a function of temperature and strain rate, and even the absolute magnitudes are quite accurate [21, 108]. In the absence of strain hardening, the alpha relaxation time in the yield plateau regime is *independent* of strain; figure 14 shows this relaxation time decreases with strain rate at various temperatures, with a tendency to converge at high rates. The inset shows the product $(\dot{\gamma}\tau_\alpha)_y$ varies with temperature and strain rate. In all cases, $(\dot{\gamma}\tau_\alpha)_y < 1$, indicating local equilibration on the segmental scale which becomes increasingly well satisfied at higher temperatures or lower strain rates.

The overall behavior in figure 14 is in good agreement with recent experiments and simulations including the ability to create master curves based on a reduced strain rate [58, 60, 108, 109]. The theory has also been worked out for, and applied to, constant stress creep and creep recovery experiments [113]. The absence of a local yield stress maximum in figure 13 reflects the fact that the calculations were performed under rapid quenching conditions where ageing and rejuvenation effects are absent. Generalization of the theory to include the latter two coupled phenomena has been recently achieved [114].

7.3. Strain hardening

At high strains, polymers massively deform resulting in a large and uniquely macromolecular increase of stress known as 'strain hardening' [4, 9, 24, 115–117]. Classic theories of strain hardening are based on a postulated analogy with the *equilibrium elasticity* of crosslinked rubber networks corresponding to dominance of an *entropic* stress of *single* strand (*intra*molecular) origin [24, 115]. Such models can fit the observed strain amplitude dependence of stress, but the underlying assumptions are highly questionable since *inter*chain forces control the yielding phenomenon. Indeed, recent experiments and simulations have shown the entropic network model is fundamentally incorrect in multiple ways [115–121]; for example, the strain hardening modulus is orders of magnitude *larger* than the rubber elasticity modulus, *increases* with cooling (not decreases as for entropic elasticity), and is deformation rate dependent. Simulations suggest the hardening modulus scales with yield stress [118]. Recent experiments [122] find the local structure of deformed glass is nearly isotropic, and affine deformation/anisotropic conformations occur only beyond a length scale ∼3–4 nm.

A segmental scale dynamical theory of strain hardening has been developed [123]. The new 'glass physics' mechanism proposed is that external deformation induces anisotropic chain conformations, which modifies interchain packing, resulting in suppression of density fluctuations and intensification of localizing dynamical constraints and activation barriers. The resulting stresses are of *inter*molecular origin.

The starting point of the theory is the strain representation of the constitutive relation, equation (46). Conformational distortion modifies the constraints encoded in the dynamical free energy. Following the ideas sketched in section 5, for a volume conserving affine uniaxial extension or compression (macroscopic deformation ratio λ) the intrachain and collective structure factors can be written as a function of deformation amplitude or true strain $\gamma = \ln(\lambda)$. Since the force correlations that determine $F_{\rm eff}(r)$ are controlled by local contributions, the dominant effect of chain anisotropy on the vertex is simply $S_0(1) \rightarrow S_0(\lambda)$, suggesting the form of the constitutive equation (to leading order) remains the same. To determine this key quantity, note that in the relevant post-yield regime the glass appears locally equilibrated, i.e. $(\dot{\gamma}\tau_\alpha)_y \ll 1$. This suggests the deformation modification of density fluctuation amplitude can be computed as in a rubber network for which PRISM theory provides a good description on length scales

below $r_X = \sqrt{N_X}\sigma$, where N_X is the number of segments between (effective) crosslinks. For glasses, r_X is identified as the scale beyond which the system is dynamically an affinely deforming solid ($r_X \sim$ 3–4 nm, $N_X \sim 16$ for PMMA [123]). The dimensionless density fluctuation amplitude then hardens (increases) under deformation as:

$$\frac{S_0(\lambda)}{S_0(1)} \simeq \frac{1}{1 + 3\sqrt{\frac{S_0(1)}{16N_X}}\left(\frac{\lambda^2+2\lambda^{-1}}{3} - 1\right)}. \quad (48)$$

The physical origin of strain hardening is suppression of density fluctuations due to anisotropic conformations and interchain packing which increases the constraining mean square forces, thereby prolonging segmental relaxation and enhancing the elastic modulus, resulting in an increase of stress. Calculations for PMMA are shown in figure 13 under compression for several temperatures and strain rates. The hardening modulus, G_R, is extracted from the slope of the stress versus rubber elasticity strain measure ($g(\lambda) \equiv \lambda^2 - \lambda^{-1}$) plot. Detailed numerical studies suggest the theoretical predictions for the magnitude, temperature, and deformation rate dependence of the hardening modulus are consistent with measurements and simulations, although much work remains to be done to fully confront the theory and experiment [123].

8. Future challenges

Much theoretical progress has occurred over the past decade in understanding both the generic and chemically-specific aspects of slow segmental dynamics in cold polymer liquids and nonequilibrium ageing and/or stressed polymer glasses. Nevertheless, the construction of a unified and comprehensive statistical dynamical theory for macromolecular materials remains in its relatively early stages. We close this article with an incomplete list of some of the critical open problems from our perspective.

(1) A fully dynamical mean field theory that can compute time correlation functions in addition to the alpha relaxation time, for realistic models of polymer chains, remains to be developed. In the spirit of multi-scale modeling, such a theory should treat the polymer as a connected sequence of elementary units that interact via effective potentials which reflect the underlying shape, stiffness and chemical diversity of real macromolecules. The role of local *intra*chain cooperativity in determining the alpha process can then hopefully be addressed in a first principles manner.

(2) Purely temporal dynamic heterogeneity effects should be elucidated for polymeric materials, especially in light of the demonstration that they result in large nonGaussian dynamical effects in colloidal suspensions and hard sphere fluids [81].

(3) Integration of the segmental relaxation theory with a description of chain dynamics on longer time and length scales is necessary to develop a full understanding of supercooled polymer melts. In particular, the 'glass-to-rubber' dynamical crossover [5, 44] remains poorly understood.

(4) More rigorous microscopic theories are needed for the origin of 'domains' (and their lifetime) in equilibrated polymer liquids that presumably underlie some dynamic heterogeneity phenomena associated with spatial variation of structure and/or thermodynamic properties. In addition to predicting domain size, its thermal dependence, and its effect on relaxation, a fundamental framework for determining correlations between the relaxation of neighboring domains is needed. The latter can be viewed as a mesoscale dynamic facilitation [31] or constraint release [5] phenomenon. Moreover, how the seemingly different mechanisms of quasi-static spatial disorder and stochastic activated hopping dynamical disorder (temporal heterogeneity) can be combined in a consistent and unified manner remains open.

(5) The temporal evolution of spatial heterogeneity and dynamical domains in quiescent nonequilibrium ageing polymer glasses needs to be understood.

(6) A full theory for the dynamically anisotropic aspects of alpha relaxation in oriented polymer liquids and deformed rubbers is needed. Extending such a theory to create a molecular scale understanding of confinement and interfacial interactions in polymer thin films and grafted polymer layers is a major challenge.

(7) A unified theory for the nonlinear mechanical response of polymer glasses should include both the average and dynamically heterogeneous physics for all the coupled competing effects that underlie the stress–strain curve in figure 4: (a) physical ageing, (b) stress-induced acceleration of relaxation, (c) post-yield 'rejuvenation' associated with mechanically-induced structural disordering, (d) high chain deformation and strain hardening. A particular challenge is to understand why in the post-yield regime the segmental dynamics appears to become far more homogeneous [58].

Finally, a new direction ripe for attack is to build on recent progress in developing microscopic theories of activated glassy dynamics in particle (colloid) and polymer systems to treat dense mixtures of flexible coils and hard nanoparticles, materials known as polymer nanocomposites [124]. Fundamental questions abound for these hybrid materials due to strong interfacial cohesive interactions between polymers and particles, large size asymmetry between species, geometric confinement effects, and the tunable complexity of spatial structure and aggregation state [125].

Acknowledgments

Our theoretical work at Illinois in the area of supercooled polymer liquids was supported by the DOE-BES program, grant no DEFG02-ER45439 via the Frederick Seitz Materials Research Laboratory. Our polymer glass work was supported by NSF-NIRT project 0505840. We gratefully acknowledge many discussions and fruitful collaborations with F T Oyerokun, M D Ediger, J J dePablo, J Caruthers and A P Sokolov, and stimulating interactions with many other scientists in the glassy dynamics field.

References

[1] Ngai K L 2000 *J. Non-Cryst. Solids* **275** 7
[2] Struick L C E 1978 *Physical Aging in Amorphous Polymers and Other Materials* (Amsterdam: Elsevier)
[3] Roland C M 2008 *Soft Matter* **12** 2316
[4] Ward I M and Hadley D M 1993 *Introduction to Mechanical Properties of Solid Polymers* (New York: Wiley)
[5] Rubinstein M and Colby R H 2003 *Polymer Physics* (Oxford: Oxford Press)
[6] deGennes P-G 1979 *Scaling Concepts in Polymer Physics* (New York: Cornell University Press)
[7] Doi M and Edwards S F 1986 *The Theory of Polymer Dynamics* (Oxford: Oxford University)
[8] McKenna G B 2003 *J. Phys.: Condens. Matter* **15** S737
[9] Meijer H and Govaert L E 2005 *Prog. Polym. Sci.* **30** 915
[10] Koshy R, Desai T, Keblinski P, Hooper J and Schweizer K S 2003 *J. Chem. Phys.* **119** 7599
[11] Angell C A, Ngai K L, McKenna G B, McMillan P F and Martin S W 2000 *J. Appl. Phys.* **88** 3113
[12] Scherer G W 1986 *Relaxation in Glass and Composites* (New York: Wiley)
[13] Adams G and Gibbs J H 1965 *J. Chem. Phys.* **43** 139
[14] Gibbs J H and DiMarzio E A 1958 *J. Chem. Phys.* **28** 373
[15] DiMarzio E A 1981 *Ann. New York Acad. Sci.* **371** 1
[16] DiMarzio E A and Yang A J 1997 *J. Res. Natl Inst. Stand. Technol.* **102** 135
[17] Moynihan C T, Easteal A J, Debolt M A and Tucker J 1976 *J. Am. Ceram. Soc.* **59** 12
[18] Eyring H 1936 *J. Chem. Phys.* **4** 283
[19] Rottler J and Robbins M O 2005 *Phys. Rev. Lett.* **95** 225504
[20] Rottler J and Robbins M O 2003 *Phys. Rev.* E **68** 011507
[21] Chen K and Schweizer K S 2007 *Europhys. Lett.* **79** 26006
[22] Vorselaars B, Lyulin A V and Michels M A J 2009 *J. Chem. Phys.* **130** 074905
[23] Warren M and Rottler J 2007 *Phys. Rev.* E **76** 031802
[24] Haward R N and Young R J 1997 *The Physics of Glassy Polymers* (London: Chapman and Hall)
[25] Debenedetti P G and Stillinger F H 2001 *Nature* **410** 259
[26] Heuer A 2008 *J. Phys.: Condens. Matter* **20** 373101
[27] Gotze W and Sjogren L 1992 *Rep. Prog. Phys.* **55** 241
[28] Chong S H and Fuchs M 2002 *Phys. Rev. Lett.* **88** 185702
[29] Dyre J 2006 *Rev. Mod. Phys.* **78** 953
[30] Langer J S 2008 *Phys. Rev.* E **77** 021502
[31] Ritort F and Solich P 2003 *Adv. Phys.* **52** 219
[32] Garrahan J P and Chandler D 2003 *Proc. Natl Acad. Sci.* **100** 9710
[33] Sollich P, Lequeux F, Hebraud P and Cates M E 1997 *Phys. Rev. Lett.* **78** 2020
[34] Lubchenko V and Wolynes P G 2007 *Ann. Rev. Phys. Chem.* **58** 235
[35] Dudowicz J, Freed K F and Douglas J F 2008 *Adv. Chem. Phys.* **137** 125
[36] Long D and Lequeux F 2001 *Eur. Phys. J.* E **4** 371
[37] Schweizer K S and Saltzman E J 2004 *J. Chem. Phys.* **121** 1184
[38] McKenna G B 1990 *Comprehesive Polymer Science* vol 2 ed C Booth and C Price (Oxford: Pergamon) p 311
[39] Bershtein V A and Ryzhov V A 1994 *Adv. Polym. Sci.* **114** 43
[40] Hansen C, Stickel F, Richert R and Fischer E W 1998 *J. Chem. Phys.* **108** 6408
[41] Novikov V N and Sokolov A P 2003 *Phys. Rev.* E **67** 031507
[42] Bassler H 1987 *Phys. Rev. Lett.* **58** 767
[43] Bohmer R, Ngai K L, Angell C A and Plazek D J 1993 *J. Chem. Phys.* **99** 4201
[44] Ngai K L and Plazek D J 1995 *Rubber Chem. Technol. Rubber Rev.* **68** 376
[45] Cangialosi D, Alegria A and Colmenero J 2009 *J. Chem. Phys.* **130** 124902
[46] Chen K and Schweizer K S 2007 *J. Chem. Phys.* **126** 014904
[47] Kunal K, Robertson C G, Pawlus S, Hahn S F and Sokolov A P 2008 *Macromolecules* **41** 7232
[48] Ding Y, Kisliuk A and Sokolov A P 2004 *Macromolecules* **37** 161
[49] Ding Y and Sokolov A P 2006 *Macromolecules* **39** 3322
[50] Boyer R F 1979 *Polym. Eng. Sci.* **19** 732
[51] Kisliuk A, Mathers R T and Sokolov A P 2000 *J. Polym. Sci. Polym. Phys.* **38** 278
[52] Pawlus S, Kunal K, Hong L and Sokolov A P 2008 *Polymer* **49** 2918
[53] Tracht U, Wilhelm M, Heuer A and Speiss H W 1999 *J. Magn. Reson.* **140** 460
[54] Sokolov A P and Schweizer K S 2009 *Phys. Rev. Lett.* **102** 248301
[55] Ilan B and Loring R F 1999 *Macromolecules* **32** 949
[56] Alcoutlabi M and McKenna G B 2005 *J. Phys.: Condens. Matter* **17** R461
[57] Loo L S, Cohen R E and Gleason K K 2000 *Science* **288** 116
[58] Lee H N, Paeng K, Swallen S F and Ediger M D 2009 *Science* **323** 231
[59] Lee H N, Paeng K, Swallen S F and Ediger M D 2008 *J. Chem. Phys.* **128** 134902
[60] Lee H N, Paeng K, Swallen S F, Ediger M D, Stamm R A, Medvedev G A and Caruthers J M 2009 *J. Polym. Sci. Polym. Phys.* **47** 1713
[61] Xia X and Wolynes P G 2000 *Proc. Natl Acad. Sci.* **97** 2990
[62] Hall R W and Wolynes P G 2008 *J. Phys. Chem.* B **112** 301
[63] Bhattacharyya S M, Bagchi B and Wolynes P G 2008 *Proc. Natl Acad. Sci.* **42** 16077
[64] Biroli G and Bouchaud J-P 2004 *J. Chem. Phys.* **121** 7347
[65] Dudowicz J, Freed K F and Douglas J F 2006 *J. Chem. Phys.* **124** 064901
[66] Dudowicz J, Freed K F and Douglas J F 2005 *J. Phys. Chem.* B **109** 21285
[67] Douglas J F, Dudowicz J and Freed K F 2006 *J. Chem. Phys.* **125** 144907
[68] Stukalin E B, Douglas J F and Freed K F 2008 *J. Chem. Phys.* **129** 094901
[69] Foreman K W and Freed K F 1998 *Adv. Chem. Phys.* **103** 335
[70] Rössler E, Hess K U and Novikov V N 1998 *J. Non-Cryst. Solids* **223** 207
[71] Merabia S and Long D 2008 *Macromolecules* **41** 3284
[72] Merabia S and Long D 2002 *Eur. Phys. J.* E **9** 195
[73] Grest G S and Cohen M H 1981 *Adv. Chem. Phys.* **48** 455
[74] Merabia S, Sotta P and Long D 2004 *Eur. Phys. J.* E **15** 189
[75] Kropka J M, Pryamitsyn V and Ganesan V 2008 *Phys. Rev. Lett.* **101** 075702
[76] Schweizer K S and Saltzman E J 2003 *J. Chem. Phys.* **119** 1181
[77] Saltzman E J and Schweizer K S 2003 *J. Chem. Phys.* **119** 1197
[78] Schweizer K S 2005 *J. Chem. Phys.* **123** 244501
[79] Kirkpatrick T R and Wolynes P G 1987 *Phys. Rev.* A **35** 3072
[80] Schweizer K S 2007 *J. Chem. Phys.* **127** 16506
[81] Schweizer K S 2007 *Curr. Opin. Colloid Interface Sci.* **12** 297
[82] Kramers H A 1940 *Physica* **7** 284
[83] Schweizer K S and Yatsenko G 2007 *J. Chem. Phys.* **127** 164505
[84] Yatsenko G and Schweizer K S 2007 *Phys. Rev.* E **76** 041506
[85] Tripathy M and Schweizer K S 2009 *J. Chem. Phys.* **130** 244907
[86] Saltzman E J and Schweizer K S 2006 *J. Chem. Phys.* **125** 044509
[87] Saltzman E J and Schweizer K S 2006 *Phys. Rev.* E **74** 061501
[88] Saltzman E J and Schweizer K S 2008 *Phys. Rev.* E **77** 051504
[89] Saltzman E J and Schweizer K S 2004 *J. Chem. Phys.* **121** 2001

[90] Saltzman E J and Schweizer K S 2007 *J. Phys.: Condens. Matter* **19** 205123
[91] Schweizer K S and Curro J G 1997 *Adv. Chem. Phys.* **98** 1
[92] Chen K and Schweizer K S 2008 *Phys. Rev.* E **78** 031802
[93] Ediger M 2000 *Ann. Rev. Phys. Chem.* **51** 99
[94] Richert R 2002 *J. Phys.: Condens. Matter* **14** R703
[95] Xia X and Wolynes P G 2001 *Phys. Rev. Lett.* **86** 5526
[96] Xia X and Wolynes P G 2001 *J. Phys. Chem.* B **105** 6570
[97] Schweizer K S and Saltzman E J 2004 *J. Phys. Chem.* B **108** 19729
[98] Lodge T P and McLeish T C B 2000 *Macromolecules* **33** 5278
[99] Oyerokun F T and Schweizer K S 2005 *J. Chem. Phys.* **123** 224901
[100] Pickett G T and Schweizer K S 2000 *J. Chem. Phys.* **112** 4869
[101] Oyerokun F T and Schweizer K S 2004 *J. Chem. Phys.* **120** 475
[102] Lubchenko V and Wolynes P G 2004 *J. Chem. Phys.* **121** 2852
[103] Merabia S and Long D 2006 *J. Chem. Phys.* **125** 234901
[104] Kovacs A J 1964 *Fortschr. Hochpolym.-Forsch.* **3** 394
[105] Chen K and Schweizer K S 2007 *Phys. Rev. Lett.* **98** 167802
[106] Stillinger F H, Debenedetti P G and Sastry S 1998 *J. Chem. Phys.* **109** 3983
[107] Kobelev V and Schweizer K S 2005 *Phys. Rev.* E **71** 021401
[108] Chen K and Schweizer K S 2008 *Macromolecules* **41** 5908
[109] Riggleman R A, Lee H N, Ediger M D and dePablo J J 2007 *Phys. Rev. Lett.* **99** 215501
[110] Riggleman R A, Schweizer K S and dePablo J J 2008 *Macromolecules* **49** 4969
[111] Osbourne M J and Lacks D J 2004 *J. Phys. Chem.* B **108** 199619
[112] Malandro D L and Lacks D J 1999 *J. Chem. Phys.* **110** 4593
[113] Chen K, Schweizer K S, Stamm R, Lee E and Caruthers J M 2008 *J. Chem. Phys.* **129** 184904
[114] Chen K and Schweizer K S, in preparation
[115] Kramer E J 2005 *J. Polym. Sci. Polym. Phys.* **43** 3369
[116] Wendlandt M, Van Beek J D, Suter U W and Meier B H 2005 *Macromolecules* **38** 8372
[117] Wendlandt M, Tervoort T A and Suter U W 2005 *Polymer* **46** 11786
[118] Hoy R S and Robbins M O 2008 *Phys. Rev.* E **77** 031801
[119] Hoy R S and Robbins M O 2007 *Phys. Rev. Lett.* **99** 117801
[120] Capaldi F M, Boyce M C and Rutledge G C 2000 *Phys. Rev. Lett.* **89** 175505
[121] Lyulin A V, Vorselaars B, Mazo M A, Balabaev N K and Michels M A 2005 *Europhys. Lett.* **71** 618
[122] Casas F, Alba-Simionesco C, Montes H and Lequeux F 2008 *Macromolecules* **41** 860
[123] Chen K and Schweizer K S 2009 *Phys. Rev. Lett.* **102** 038301
[124] Winey K I and Vaia R 2007 *MRS Bull.* **32** 314
[125] Hooper J B and Schweizer K S 2005 *Macromolecules* **38** 8858